

# Measuring Cytoskeletal Mechanical Fluctuations and Rheology with Active Micropost Arrays

Yu Shi,<sup>1,3</sup> Shankar Sivarajan,<sup>1</sup> John C. Crocker,<sup>2</sup> and Daniel H. Reich<sup>1,4</sup>

<sup>1</sup>Department of Physics and Astronomy, Johns Hopkins University, Baltimore, Maryland

<sup>2</sup>Department of Chemical and Biomolecular Engineering, University of Pennsylvania, Philadelphia, Pennsylvania

<sup>3</sup>Current address: Department of Biomedical Engineering, University of North Carolina, Chapel Hill, North Carolina

<sup>4</sup>Corresponding author: [reich@jhu.edu](mailto:reich@jhu.edu)

The dynamics of the cellular actomyosin cytoskeleton are crucial to many aspects of cellular function. Here, we describe techniques that employ active micropost array detectors (AMPADs) to measure cytoskeletal rheology and mechanical force fluctuations. The AMPADs are arrays of flexible poly(dimethylsiloxane) (PDMS) microposts with magnetic nanowires embedded in a subset of microposts to enable actuation of those posts via an externally applied magnetic field. Techniques are described to track the magnetic microposts' motion with nanometer precision at up to 100 video frames per second to measure the local cellular rheology at well-defined positions. Application of these high-precision tracking techniques to the full array of microposts in contact with a cell also enables mapping of the cytoskeletal mechanical fluctuation dynamics with high spatial and temporal resolution. This article describes (1) the fabrication of magnetic micropost arrays, (2) measurement protocols for both local rheology and cytoskeletal force fluctuation mapping, and (3) special-purpose software routines to reduce and analyze these data. © 2022 The Authors. Current Protocols published by Wiley Periodicals LLC.

**Basic Protocol 1:** Fabrication of magnetic micropost arrays

**Basic Protocol 2:** Data acquisition for cellular force fluctuations on non-magnetic micropost arrays

**Basic Protocol 3:** Data acquisition for local cellular rheology measurements with magnetic microposts

**Basic Protocol 4:** Data reduction: determining microposts' motion

**Basic Protocol 5:** Data analysis: determining local rheology from magnetic microposts

**Basic Protocol 6:** Data analysis for force fluctuation measurements

**Support Protocol 1:** Fabrication of magnetic Ni nanowires by electrodeposition

**Support Protocol 2:** Configuring Streampix for magnetic rheology measurements

Keywords: cytoskeleton • magnetic actuation • microposts • microrheology

**How to cite this article:**

Shi, Y., Sivarajan, S., Crocker, J. C., & Reich, D. H. (2022). Measuring cytoskeletal mechanical fluctuations and rheology with active micropost arrays. *Current Protocols*, 2, e433. doi: 10.1002/cpz1.433

**INTRODUCTION**

The mechanics of the actomyosin cytoskeleton is crucial to many aspects of cellular function, and the study of its dynamics is critical to advancing the understanding of mechanobiology. The cytoskeleton is an active material that can generate forces internally from the action of myosin motors. It is thus essential to characterize both its rheological properties and the dynamical fluctuations of the forces generated in its various component structures, such as stress fibers and the cortex. A variety of approaches are available to measure cellular mechanical properties, including atomic force microscopy (Hecht et al., 2015; Kilpatrick, Revenko, & Rodriguez, 2015; Li, Dang, Liu, Xi, & Wang, 2017; Smith, Tolloczko, Martin, & Grutter, 2005), magnetic twisting cytometry (Fabry et al., 2001; Massiera, Van Citters, Biancaniello, & Crocker, 2007), and active microrheology using internalized probe particles (Wei et al., 2008; Hoffman, Massiera, Van Citters, & Crocker, 2006). Quasi-static cellular force generation (e.g., traction forces and contractility) is commonly measured by techniques such as traction force microscopy (Plotnikov, Sabass, Schwarz, & Waterman, 2014) and micropost array detectors (MPADs) (du Roure et al., 2005; Geng & Wang, 2016; Tan et al., 2003), but as commonly applied, these techniques have not enabled access to cytoskeletal force fluctuations. There is growing recognition, however, of the importance of measuring the active dynamics and mechanics of cytoskeletal traction force processes such as during cell spreading (Lohner et al., 2019; Wolfenson et al., 2016) and in recently observed rearrangements in the actomyosin cortex termed cytoquakes (Alencar et al., 2016; Floyd, Levine, Jarzynskie, & Papoian, 2021; Shi et al., 2021; Shi, Porter, Crocker, & Reich, 2019). Passive microrheology on internalized probe particles (Guo et al., 2014) or cellular organelles (Lau, Hoffman, Davies, Crocker, & Lubensky, 2003) can give information on the spectrum of cytoskeletal force fluctuations. However, it is not always clear what portion of the cytoskeleton is being probed. Furthermore, number of probes that can be embedded may be limited, limiting the ability to map spatial variations in force fluctuations.

In this protocol, we describe the fabrication and use of active micropost array detectors (AMPADs), which are MPAD devices with magnetic nanowires embedded in a subset of the microposts to enable the actuation of those posts for studies of the local rheology of the cytoskeleton. Techniques are described to track the microposts' motions with nanometer precision at high speed to enable measurements of the local cellular rheology at well-defined positions. When applied to the full array of microposts in contact with a cell, high-precision tracking techniques also allow mapping of the cytoskeletal mechanical fluctuation dynamics with unprecedented spatial and temporal resolution.

The techniques described in this article are organized into six basic protocols, as outlined in Figure 1. Approaches for producing poly(dimethylsiloxane) (PDMS) MPAD arrays via replica molding have been described in detail (Fu et al., 2010; Tan et al., 2003; Weng & Fu, 2011; Yang, Fu, Wang, Desai, & Chen, 2011), and so Basic Protocol 1 describes only the key additional steps for producing AMPAD arrays with embedded magnetic Ni nanowires. We then focus on the high-speed measurement techniques and associated data analysis approaches needed to study cytoskeletal rheology and mechanical fluctuations. Basic Protocol 2 describes data acquisition for cellular force fluctuations on

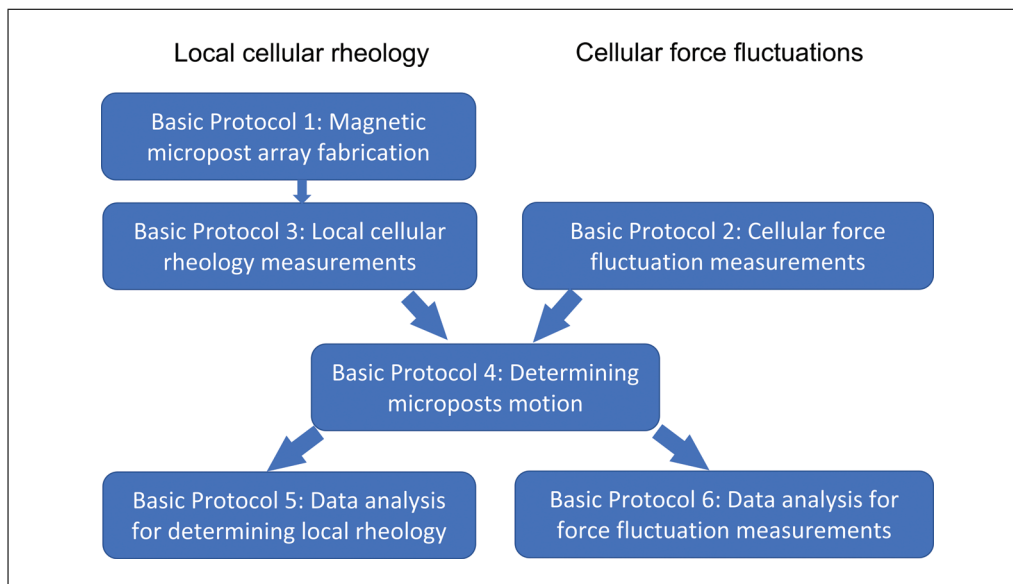


**Figure 1** Overview of protocols and workflow for local cellular rheology and force fluctuation measurements using AMPADs.

non-magnetic micropost arrays. Basic Protocol 3 describes data acquisition for local cellular rheology measurements with magnetic microposts. Basic Protocol 4 illustrates the use of high-resolution particle tracking techniques (Crocker & Grier, 1996) to extract the microposts' positions versus time for both magnetic and non-magnetic posts. Basic Protocol 5 describes converting such data for magnetic posts to frequency-dependent local cellular rheology. Basic Protocol 6 describes the analysis of the motion of non-magnetic posts, focusing on the posts' mean squared displacements (MSDs) to yield maps of the fluctuations and identify those posts coupled to different components of the cytoskeleton such as the stress fibers and the actomyosin cortex. Support Protocol 1 describes the fabrication of magnetic nanowires via electrodeposition in nanoporous templates. Support Protocol 2 describes how to configure the specific video acquisition software (Streampix) we employ for the magnetic rheology measurements. Note that Basic Protocols 4–6 are described in the context of special-purpose software written in Igor Pro (Wavemetrics) (available as an online resource on Github). However, overviews of the principles involved are also provided should researchers wish to implement these protocols in other programming environments.

## FABRICATION OF MAGNETIC MICROPOST ARRAYS

This protocol uses replica molding techniques to fabricate PDMS micropost arrays with magnetic Ni nanowires embedded in individual microposts. These nanowires have diameters of 350 nm, lengths of 5  $\mu\text{m}$ , and average low-field magnetic moments  $\mu = 0.15 \text{ pA m}^2$ , aligned along their long axes (Hultgren et al., 2005; Hultgren, Tanase, Chen, & Reich, 2004). This protocol assumes the user can follow published protocols to make, or has access to, “master” versions of the arrays, which are typically made on silicon wafers by photolithographic techniques (Fu et al., 2010; Yang et al., 2011), and has followed published methods to cast “negative” PDMS molds of the desired micropost arrays (Tan et al., 2003; Yang et al., 2011). To make magnetic micropost arrays, magnetic Ni nanowires are positioned in the post forms (holes) in the negative molds. PDMS is then cast around them, embedding the nanowires in the posts. The nanowires must be shorter than the length of the microposts, or the magnetic microposts may be too stiff to bend in response to magnetic torques applied to the nanowires. The procedures described will yield approximately 1% of the posts containing magnetic nanowires for post arrays with 1.8  $\mu\text{m}$  post diameters and 4  $\mu\text{m}$  center-to-center post spacing (Shi et al., 2019). Note

## BASIC PROTOCOL 1

Shi et al.

3 of 47

that the magnetic microposts will be randomly distributed within the arrays. After the arrays are fabricated, they are removed from the molds in ethanol and dried using a critical point dryer to avoid collapsing the posts (Yang et al., 2011). The tips of the posts are functionalized with the extracellular matrix protein fibronectin via microcontact printing to promote cell adhesion to the micropost tips (Tan et al., 2003; Yang et al., 2011). Fibronectin works well for various cell types, but other ECM proteins can be used if needed. The sides of the posts and the regions in between are then blocked from cell adhesion by coating with Pluronic F-127. This is important as the conversion of micropost deflection to force depends on the cells' forces being restricted to the posts' tips (Fu et al., 2010; Tan et al., 2003). We note that non-magnetic micropost arrays, produced via published protocols (Yang et al., 2011), are also used for some of the measurements described below.

### Materials

Poly(dimethylsiloxane) (PDMS) and curing agent (Sylgard 184, Dow Corning)  
Tridecafluorooctyltrichlorosilane (T2492, UCT Specialties)  
100% ethanol  
Magnetic Ni nanowires suspended in ethanol ( $10^6$  nanowires/ml; see Support Protocol 1)

Small metal spatula  
50-ml centrifuge tubes  
Centrifuge (Thermo Centra CL2, or equivalent)  
50-mm square polystyrene weighing dishes (Southern Labware, or equivalent)  
Vacuum desiccator (Bel-Art Products)  
Vacuum pump for degassing PDMS (Ningbo Maisi Model TC-100, or equivalent)  
70°C Oven (VWR ShelLab Model 1310, or equivalent)  
Oxygen plasma etcher (Technics PE II-A, or equivalent)  
Vacuum desiccator for silanization (Bel-Art Products)  
Vacuum pump for silanization (FJC Products, Model VP 5.0, or equivalent).  
Standard cover glasses (22 mm × 22 mm)  
UV/Ozone treater (UVO Cleaner Model 42, Jelight)  
Plastic Petri dishes (Fisherbrand 100 mm × 15 mm polystyrene)  
Tweezers (metal, Techni-Tool)  
Ultrasonic agitator (Branson 1510, or equivalent)  
Vortex shaker (VWR model 100, or equivalent)  
Micropipette, 200 µl capacity (Eppendorf Research, or equivalent)  
200 µl pipette tips (USA Scientific TipOne)  
Rectangular rare-earth magnets with their magnetic poles perpendicular to the large faces (K&J Magnetics BC-82; Dimensions 1.9 cm × 1.3 cm × 0.32 cm ( $\frac{3}{4}$ " ×  $\frac{1}{2}$ " × 1/8"))

1. Treat the molds with an oxygen plasma under a pressure of 450 mTorr at 100 W power for 90 s.

*This is to enable the functionalization of the mold surfaces in step 2. It must be done before a mold is used for the first time and should be repeated every 3-5 times a mold is used.*

2. Transfer the molds to a vacuum desiccator with a few drops of tridecafluorooctyltrichlorosilane on a glass coverslip. Pump to a rough vacuum and let stand overnight.

*This enables the separation of the PDMS micropost arrays from the molds. This only needs to be done every 3-5 times a mold is used.*

3. Select a pre-prepared solution of nanowires of the desired dimensions at a concentration of  $10^6$  /ml in ethanol.

*The nanowires must be shorter than the length of the microposts, or the magnetic microposts may be too stiff to bend in response to magnetic torques applied to the nanowires.*

4. Sonicate the nanowire solution for 5 min.

5. Agitate the nanowire suspension in a vortex shaker for a few seconds.

*The goal of these two steps is to break up any clumps of nanowires that may have formed due to magnetic attraction between the nanowires.*

6. Arrange PDMS molds in a plastic Petri dish (one mold per array desired).

7. Place rectangular rare-earth magnets under the Petri dish, one under each mold.

*The magnets should be placed flat with their North or South poles pointing up. These magnets should remain under the molds until the molds have been filled with PDMS and are placed in the oven to be cured to keep the nanowires aligned vertically.*

8. Pipette 30  $\mu$ l of nanowire solution onto each mold.

*The magnets underneath the molds will align the nanowires vertically in suspension and pull them into the holes in the mold that will form the microposts. If the nanowires are not aligned in this manner, they will not go into the post holes but will lie horizontally on the tops of the molds.*

9. Wait for the solution to evaporate (20-30 min).

*This prevents nanowires from flowing off the molds when the next drop is added.*

10. Pipette another 30  $\mu$ l of nanowire solution onto each mold and wait for it to evaporate.

11. Repeat until 180  $\mu$ l of nanowire solution has been pipetted onto each mold.

*This should yield arrays with  $\sim$ 1% of the microposts containing nanowires.*

12. Mix PDMS and curing agent in a 10:1 ratio in a Styrofoam cup.

*Steps 12-15 can be done while waiting for the nanowire solution to evaporate from the molds (steps 9-11). Prepare about 20 g of the PDMS mixture (e.g., use 20 g of PDMS and 2 g of curing agent.)*

13. Stir the mixture with a spatula for about 3-4 min.

*Stir until the bubbles disappear.*

14. Pour the mixture into a 50-ml centrifuge tube and centrifuge for 5 min at  $10^4$  m/s<sup>2</sup> (5k rpm on the above system).

*This is to degas the PDMS to eliminate bubble formation that can lead to defects in the micropost structures.*

15. Arrange cover glasses (one for each micropost array desired) on a plastic Petri dish and treat with ultraviolet (UV)/ozone for 7 min.

*This oxidizes the surface of the glass to promote the bonding of PDMS.*

16. Add a drop of PDMS to each mold from step 11.

*The magnets should still be under the dish containing the molds.*

17. Press a UV-treated cover glass onto each of the molds.

18. Degas the molds in a vacuum desiccator for 5 min.

19. Bake the molds at 65°C on a hot plate for 1 hr.

*This hardens the PDMS microposts sufficiently so that the nanowires do not move during subsequent processing.*

20. Remove the magnets.  
*Do not put the magnets in the curing oven.*
21. Flip the molds over so the cover glasses are on the bottom.
22. Bake the dish with the cover glasses in a curing oven set to 70°C overnight.  
*This cures the PDMS. Keep the Petri dish level so the molds do not slide off the PDMS before it cures.*
23. Remove the Petri dish and devices from the oven, allow to cool, and add 100% ethanol to the dish until the cover glasses are completely immersed.  
*The molds do not need to be completely immersed.*
24. Use tweezers to twist the molds off the cover glasses.  
*Keep the cover glasses with the MPAD arrays immersed in ethanol during this process.*  
*At this stage, the physical fabrication of the magnetic MPADs is complete. In subsequent handling, care must be taken not to damage the micropost arrays. In particular, arrays that are wet (e.g., in ethanol, water, or PBS) must not be allowed to dry out as the surface tension of the drying front can knock down the microposts. A critical point dryer must be used to dry the arrays.*
25. Dry the arrays in a critical point dryer  
*This procedure is described in (Yang et al., 2011).*
26. Stamp fibronectin on the post tips via micro-contact printing and coat the non-stamped regions of the arrays with F127 Pluronic.  
*This will promote cell adhesion to the post tips rather than the sides of the posts and other surfaces of the arrays. This is important as the conversion of post deflections to force depends on the assumption that cells are adherent only to the post tips. Procedures for these steps are described in Yang et al., 2011.*
27. Store fibronectin and Pluronic coated arrays in PBS until used.  
*Arrays should be used within 24 hr after coating to avoid deterioration of the fibronectin coatings.*

**SUPPORT  
PROTOCOL 1**

**FABRICATION OF MAGNETIC NI NANOWIRES BY  
ELECTRODEPOSITION**

This protocol describes the fabrication of the nickel nanowires used to make the microposts magnetic. The nanowires are made by electrodeposition in nanoporous templates (Felton, 2009; Hultgren et al., 2005; Kramer, 2009; Rovner, 2013). The templates are commercial 60- $\mu\text{m}$  thick alumina filter membranes. These membranes have nominal pore diameters of 100 nm but only have this diameter in a small region 3-5  $\mu\text{m}$  thick near the bottom of the membrane. For most of their length, their diameter is 350 nm, which sets the diameter of the nanowires. The length of the nanowires is controlled by how much Ni is deposited into the pores. For the microposts described in this protocol, the desired nanowire length is 5  $\mu\text{m}$ . (The deposition procedure typically allows the length to be controlled to  $\pm 10\%$ .) A copper film is sputter-deposited onto the bottom of the filter membranes to seal the ends of the pores in the template and serve as a working electrode for the electrodeposition. Note that thermal evaporation of Cu has been found inadequate to seal the pores. A thin layer of Cu is electrodeposited first to fill the narrow (100 nm diameter) end sections of the pores, and then Ni is deposited to produce the desired magnetic nanowires. The Cu is removed using a copper etchant, and the template is dissolved in KOH to release the nanowires. The wires may be stored for extended periods in ethanol or isopropanol before use.

## Materials

Alumina filter membranes, nominal pore size 100 nm, 60  $\mu\text{m}$  thickness (Anodisc 47, Whatman)  
Copper sputter target  
Argon gas  
Acetone  
Isopropanol  
Cu plate, 0.25" thick, approx. 2.5" square  
DI water  
Copper electrodeposition solution: 125 g/L  $\text{CuSO}_4 \cdot 5\text{H}_2\text{O}$ , 30 g/L  $\text{H}_3\text{BO}_3$ , 20 g/L NaCl in DI water.  
Nickel electrodeposition solution: 514 g/L  $\text{Ni}(\text{SO}_3\text{NH}_2)_2 \cdot 4\text{H}_2\text{O}$ , 20 g/L  $\text{NiCl}_2 \cdot 6\text{H}_2\text{O}$ , 20 g/L  $\text{H}_3\text{BO}_3$  in DI water.  
0.5 M KOH solution in DI water

Glass vials or glass test tubes  
Sputter deposition system  
Teflon electrodeposition chamber (cylinder with open bottom)  
Spring clamp  
Blow torch  
Pt counter electrode, consisting of Pt mesh attached to a Pt wire  
Ag/AgCl reference electrode (Bioanalytical Systems, Inc. MF-2052)  
Potentiostat (Princeton Applied Research, model 263A or equivalent)  
Computer to control potentiostat  
Single-edge razor blades  
Temperature-controlled water bath (Neslab RTE-211, or equivalent)  
Sonicator (Branson 1510, or equivalent)

1. Clean alumina templates by rinsing in acetone and isopropanol.
2. Sputter deposit a layer of Cu 500 nm thick on the side of the alumina templates with the nominal pore diameter (the back side).

*The exact procedures will depend on the details of the sputtering system used but will typically be done in 5 mTorr of argon gas. A sputtering current of 50 mA and a deposition time of 25 min yielded the desired layer thickness in our system. This layer should not be too thick to facilitate its removal at the end of the nanowire fabrication procedure. If this layer is too thick, Cu will adhere to the tips of the nanowires, or the alumina will not be completely dissolved.*

3. Rub one side of the Cu plate thoroughly with sandpaper to remove its surface oxide.

*This provides a clean surface to make good electrical contact with the Cu film on the template.*

4. Rinse the Cu plate with DI water.
5. Place the filter template Cu-side down on the Cu plate.
6. Rinse a rubber o-ring with DI water and place it on the top of the filter template.

*The o-ring should be sized to the diameter of the deposition chamber.*

7. Place the Teflon electrodeposition chamber on the o-ring and clamp it to the Cu plate with a spring clamp.

*The electrodeposition chamber should have the form of a hollow cylinder, as the bottom is formed by the filter template and the Cu plate, which together serve as the working electrode. A good seal must be formed by the o-ring so that with the filter template/Cu*

*plate forming the bottom of the electrodeposition chamber, no liquid can leak out. A flange on the bottom end of the Teflon tube to allow mating to the spring clamp is helpful.*

8. Rinse the chamber with DI water.
9. Fill the chamber with Cu electrodeposition solution.
10. Preclean the Pt counter electrode by placing it briefly in the flame of a blow torch and then washing it in DI water.
11. Insert an Ag/AgCl electrode in the deposition solution to serve as a reference electrode.
12. Connect the Pt electrode, Ag/AgCl reference electrode, and the Cu plate to the potentiostat.
13. Deposit Cu to fill the bottom 3-5  $\mu\text{m}$  of the pores, using a reference potential of  $-0.2\text{ V}$ .

*For the diameter of our deposition chamber, approximately 1 Coulomb of copper deposits 1  $\mu\text{m}$  in the pores. The goal is to fill the bottom, thinner section of the pores.*

14. Pour off the spent Cu deposition solution and rinse the deposition chamber and electrodes in DI water to remove any remaining electrolytes.
15. Fill the chamber with the Ni deposition solution.
16. Deposit Ni into the pores to the desired length of the nanowires, using a reference potential of  $-1\text{ V}$ .

*For the microposts we typically use, the desired length is 5  $\mu\text{m}$ . In our deposition system, we find deposition rates of 2-3  $\text{C}/\mu\text{m}$  of Ni in the pores.*

17. Pour off the spent Ni deposition solution and rinse the deposition chamber and electrodes in DI water.
18. Remove the filter membrane from the apparatus.
19. Cut away the sections of the filter template that were not electrodeposited with a razor blade.
20. Place the section of the filter membrane containing the nanowires in a Petri dish, Cu side up.
21. Rub the filter membrane with a Q-tip soaked in a Cu etching solution to remove the Cu. Repeat until all traces of the Cu are gone.

*This process can take 20-30 min and will require multiple Q-tips. The template should turn completely black when all the Cu is removed.*

22. Place the template with the nanowires in a glass vial or test tube.
23. Fill the vial (or test tube) with 0.5 M KOH in water.

*KOH will dissolve the alumina of the filter membranes but will not affect the Ni nanowires.*
24. Seal the vial with parafilm and place the vial in a water bath at  $60^\circ\text{C}$  for 4-6 hr or overnight.
25. Sonicate the vial and nanowire suspension for 10 min.

*This will help break up clumps of filter material and nanowires.*
26. Place one or more rare earth magnets against the side of the vial for  $\sim 5$  min.



*This will collect the nanowires by attracting them to the magnet. The magnet should immobilize the nanowires against the inside wall of the vial.*

27. Decant the KOH solution and replace it with a fresh KOH solution while keeping the magnet against the side of the vial.

*The magnet must not move from its position on the side of the vial during these steps, or nanowires may be lost when the solution is decanted. The magnet may be taped to the vial, or a collar that holds the magnet and fits tightly around the vial may be constructed.*

28. Reseal the vial with parafilm and place the vial in a water bath at 60°C for another 4-6 hr.
29. Sonicate the vial for 10 min and shake gently by hand.
30. Collect and immobilize the nanowires again by placing one or more rare earth magnets against the side of the vial for ~5 min.
31. Decant the solution and replace it with DI water to wash the nanowires.
32. Repeat steps 29-31 five times.
33. Collect and immobilize the nanowires again.
34. Decant the DI water and rinse the nanowires once in acetone.
35. Repeat step 30 and replace the acetone with ethanol.

*The nanowires may be stored in ethanol for extended periods, up to several years, while still retaining their magnetic properties.*

36. Inspect the nanowires with an SEM or an optical microscope after fabrication.

*Nanowires can be prepared on a microscope slide for optical imaging by allowing a drop of ethanol-containing nanowires to evaporate. The diameter of the nanowires cannot be resolved by standard optical microscopy, but the lengths of the wires can be assessed. For SEM imaging, evaporate a drop of ethanol containing nanowires on a conducting substrate. The nanowires should form rods of uniform diameter. We analyzed SEM images and found that the average diameter of nanowires produced in these templates is  $350 \pm 4$  nm (Tanase et al., 2005).*

## **DATA ACQUISITION FOR CELLULAR FORCE FLUCTUATIONS ON NON-MAGNETIC MICROPOST ARRAYS**

This protocol describes how to use video microscopy to measure the time-dependent displacements of microposts in contact with cells. The resulting data are of sufficient quality that the positions of the microposts can be measured with nanometer accuracy at up to 100 video frames per second, using the image analysis procedures described in Basic Protocol 4. This protocol is used for data acquisition for cellular force fluctuations on non-magnetic micropost arrays. Many of the steps described here are also needed for local cell rheology measurements with magnetic micropost arrays (Basic Protocol 3.) This protocol includes instructions for seeding and culturing cells on the micropost arrays before the measurements. These are, of necessity, somewhat generic and may have to be modified depending on the specific cell type used. When imaging a cell, it is important to have it sufficiently centered in the field of view to have a border of at least 3-4 rows and columns of microposts that are not engaged with the surrounding cell. Data from these “background” microposts are used in the data reduction (Basic Protocol 4) to compensate for any overall drift in the array’s position and to determine the undeflected positions of the posts in contact with the cell. The data from the background posts also provide a measure of imaging noise in the system. Note that in this protocol, there will be a free liquid-air interface from the cell culture medium to the optical path. This has not proven

to be a problem for experiments such as those described in (Shi et al., 2019; Shi et al., 2021). However, if needed, it is possible to eliminate this potential source of noise in the post tracking by using a dish such as that described in Basic Protocol 3 that eliminates the liquid-air interface.

### **Materials**

Micropost arrays, functionalized to promote cell adhesion on the post tips, as described in Basic Protocol 2.

Cells in culture ready to be passaged

Cell culture medium with serum, antibiotics, etc., to culture cells under study.

Disposable, sterile 5 and 1 ml pipettes (Falcon, ThermoFisher, etc.)

5% premixed CO<sub>2</sub> gas

Biosafety cabinet (Labconco Purifier BSC Class II, or equivalent)

Glass-bottomed P35 culture dishes (Thermo Scientific)

Sterilized tweezers

Pipettor (Falcon Express)

Tissue culture incubator (Sanyo Model MCO-17A, or equivalent)

Cell culture inspection microscope (Nikon TS-100, or equivalent)

Inverted microscope (Nikon TE-2000E or equivalent)

10×, NA = 0.3 air objective (Nikon Plan Fluor)

40×, NA = 0.6, extra-long working distance air objective with correction collar (Nikon Plan Fluor).

100 W halogen illuminator

long-working distance condenser with NA = 0.52.

Ultraviolet (UV) (Edmund Optics cat. no. 64-667) and infrared (Edmund Optics cat. no. 47-303) filters

Microscope enclosure incubator with an on-stage environmental chamber (In Vivo Scientific, Model CH.HC5.SAT, or equivalent)

Microscope stage heating plate (20/20 Technologies, Model TC-500, or equivalent)

Computer equipped with hardware to support Norpix Streampix software and camera

Norpix Streampix software (Version 5.16 or later)

Gigabit Ethernet camera (Allied Vision GX1050, or equivalent)

### **Seeding cells onto an MPAD array**

1. Prepare a cell suspension in culture medium.

*This procedure should be identical to the one used for routine passaging. Using appropriate sterile techniques, all steps should be carried out in a biosafety cabinet.*

2. Preheat to 37°C and add 2 ml cell culture medium to a glass-bottom P35 culture dish.

*This should be the regular medium used to culture the cells, including any standard serum and antibiotics.*

3. Transfer an MPAD array from PBS to the P35 dish with tweezers.

4. Pipette 200 µl of cells in suspension at the desired concentration into the dish.

*The above steps are the same as routine passaging, but with cells transferred to the MPADs instead of a new culture dish. The goal is to have a sufficiently sparse population of cells on the MPAD array to measure individual, isolated cells. This step will have to be calibrated for each cell type to account for its propensity to adhere to the microposts.*

5. Inspect the culture dish with a microscope.

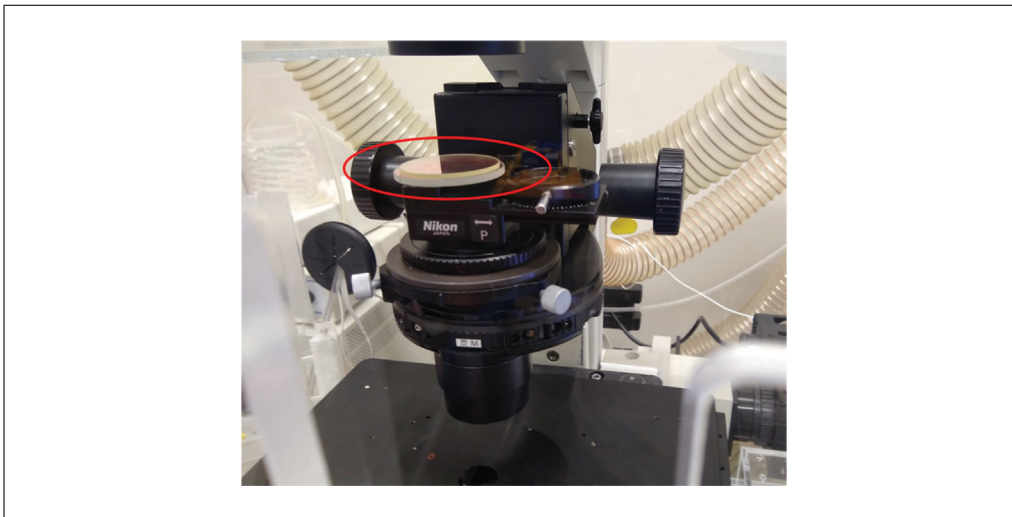


**Figure 2** Condenser of Nikon TE-2000 microscope, showing location of UV and IR filters in the incident light path (glass disks circled in red.).

*When using a 10× objective focused on the top of the microposts, between 10 and 30 floating cells should be visible and sparsely distributed across the field of view.*

6. Incubate MPADs overnight in a tissue culture incubator at 37°C and the CO<sub>2</sub> level appropriate for the cells in use.

*Check that the cells are well-spread and adhered to the arrays before proceeding.*

7. Remove air bubbles from under the MPAD using tweezers.

*Lift the MPAD just off the bottom of the dish and press it back into place. This is necessary to keep the MPADs from sliding.*

#### **Data acquisition**

8. Switch on the hot plate and microscope stage and allow to equilibrate at 37°C.
9. Put the environmental chamber onto the stage and connect it to the airflow control unit.
10. Start the flow of 5% premixed CO<sub>2</sub> with an influx of 200 cm<sup>3</sup>/min.
11. Transfer the dish with cells seeded on an MPAD to the microscope's incubator and place it in the environmental chamber.
12. Wait until the medium in the dish warms to 37°C.

*This should take about 20 min.*

13. Position the UV and infrared filters in the incident light path of the microscope (Fig. 2) and switch on the illuminator. Position the microscope's green interference filter (GIF) in the light path.

*This confines the illumination to visible wavelengths and allows high illumination intensities while avoiding cell damage through prolonged exposure. The GIF further optimizes the incident light in the region of the best performance of standard white-light lenses.*

14. Open the condenser aperture fully and ensure no other optical elements, such as phase rings, are in the light path through the condenser.

*This is to maximize spatial resolution when imaging the microposts.*

15. Adjust the microscope for Kohler illumination.

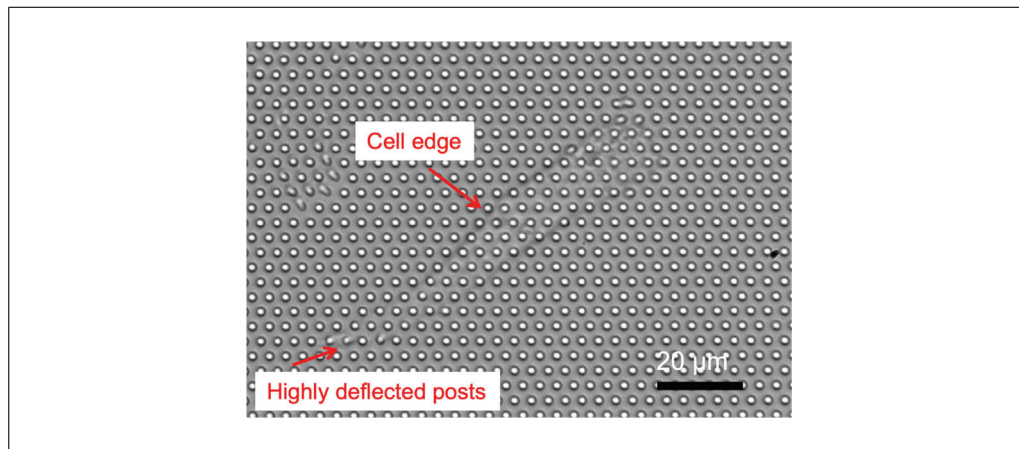


**Figure 3** 40× image of a NIH 3T3 cell on a micropost array.

16. Using a 10× objective, center the field of view on a cell.
17. Rotate the sample dish so that rows of posts (in the hexagonal grid) are aligned with the horizontal (x translation axis) of the microscope stage (see Fig. 3).

*This is most easily done with a 10× objective. The analysis software needs the post arrays to be in this orientation, and it is important to minimize the amount of image rotation required.*

18. Switch to the 40× objective.
19. Switch on the camera in the Norpix software.
20. Focus the camera on the plane of the tips of the posts (see Fig. 3).

*If needed, rotate the camera so that the horizontal rows of posts are aligned with the x-axis of the camera's image. The circular outlines of the post tips should be sharp. This imaging mode is optimized to observe the post tips and not the cells, so it can be somewhat difficult to see the precise outline of a cell. However, as shown in Figure 3, the approximate outline can be discerned, and highly deflected posts near the cell's edges can sometimes be seen.*

21. Optimize the image quality using the objective's correction collar.

*This adjustment may be needed to compensate for aberration as one is imaging through both the glass bottom of the culture dish and the coverslip on which the MPAD array is mounted.*

22. Set the gain to 1 in Norpix to avoid amplifying camera noise, and set the exposure time [Live Adjustments > Grabber Properties > Exposure (μs)]. Increase the illuminator intensity to maximize image intensity without saturating the image.

*Examine the histogram of the current frame, load Norpix's "histogram" module, and adjust the illuminator intensity until the high-intensity tail of the histogram just reaches the camera's maximum pixel intensity (e.g., 255 for an 8-bit image) (Fig. 4). This should correspond to the bright spots at the centers of the posts. For our system, we use an exposure time of 4.5 ms for recordings at 100 fps.*

23. Record the cell at 100 fps for the desired time. In Norpix, these images are saved as lossless AVI files.

*We typically image the cells for 30 min each since the phenomena we are interested in occur on that timescale. If the size of the resultant movies becomes a problem, the frame rate can be reduced but at the cost of a loss of time resolution and a more limited ability to account for background noise.*

24. Change the field of view to center on another cell and repeat for as many cells as needed.

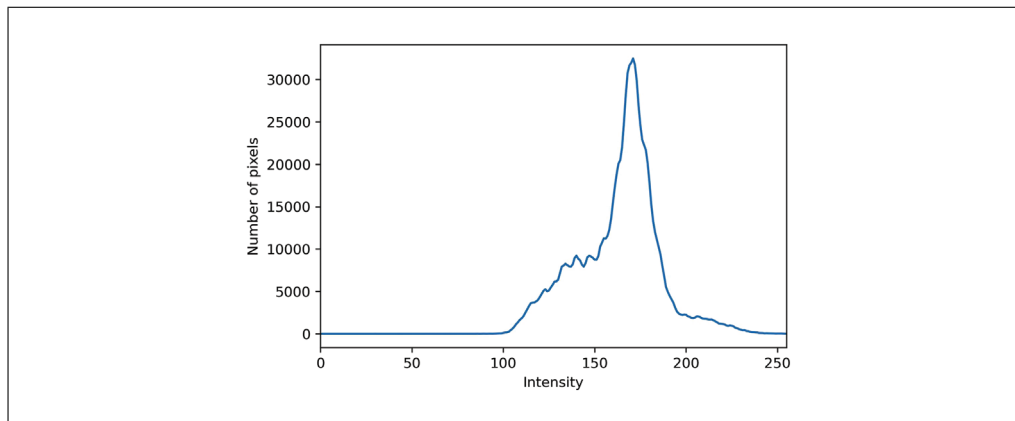


**Figure 4** Sample histogram of image intensity after setting halogen illuminator lamp intensity in Streampix prior to data acquisition.

## DATA ACQUISITION FOR LOCAL CELLULAR RHEOLOGY MEASUREMENTS WITH MAGNETIC MICROPOSTS

## BASIC PROTOCOL 3

This protocol describes measurements of the local rheology of a cell by actuating a magnetic micropost with an AC magnetic field and recording the resulting motion of the post. For the Ni nanowires described here, this requires the ability to apply an AC magnetic field in the range of 10 mT to ensure a linear response. The system described operates from 0.1 Hz to over 100 Hz to enable robust measurement of the frequency-dependent rheology. It employs a dual magnetic tweezer (Fig. 5) to ensure that only one cell is exposed to the magnetic field at a time, but if this is not a consideration, then alternative approaches may be employed to generate the needed field. Detailed information on the construction of a magnetic tweezer system is provided in several publications (Bose, Huang, Eyckmans, Chen, & Reich, 2018; Kramer, 2009; Lin, Kramer, Chen, & Reich, 2012; Zhao, Boudou, Wang, Chen, & Reich, 2014).

A block diagram of the magnetic actuation and video microscopy measurement system is shown in Figure 6. A PC running the Streampix (Norpix, version 5.16) video acquisition software is equipped with a National Instruments (NI) DAQ card. To produce the AC magnetic field, sinusoidal voltage waves from the NI card provide programming voltages to a Kepco BOP AC power supply operating in current-control mode, which provides current to drive a dual magnetic tweezer system mounted on an inverted microscope (green arrows). Hall sensors at the back end of the tweezers' cores monitor their magnetic field, and the Hall voltages are read by the DAQ card and recorded by the PC (red arrow). The PC also controls a CCD camera on the microscope, recording the microposts' motion (black arrow). To ensure the Hall voltages are measured simultaneously with the video frames, digital pulses from the camera when each frame is captured are used to trigger the measurements of the Hall sensors by the NI card (yellow arrow).

### Materials

Gibco CO<sub>2</sub> independent culture media (Thermo Fisher cat. no. 18045088)

5% Trypsin-EDTA (Corning)

PBS

Biosafety cabinet (Labconco Purifier BSC Class II, or equivalent)

Magnetic tweezers: two solenoids filled with iron cores, mounted on 3-axis micromanipulator stages

Sample dish with indented lid; custom-built, details provided below

PDMS ring to seal sample dish; details provided below

Computer configured to support Streampix software and equipped with National Instruments PCIe-6231 DAQ card

Shi et al.

13 of 47

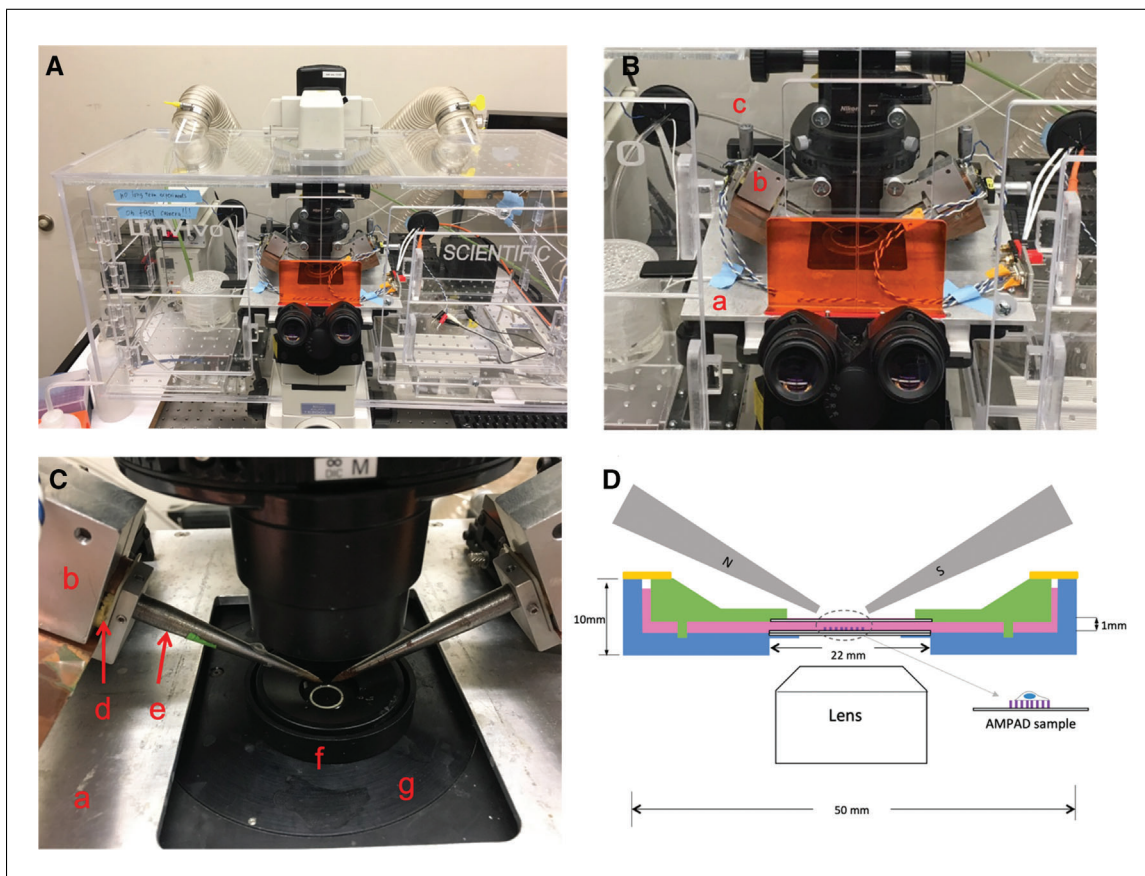


**Figure 5** Dual magnetic tweezer system mounted on Nikon T/E 2000 microscope. **(A)** Microscope in enclosure incubator. **(B)** Closeup showing tweezer assembly mounted on metal plate (a) over microscope stage. Each of the two magnet assemblies is mounted in an aluminum heat-sinking block (b) on a 3-axis micromanipulator (c). **(C)** Further closeup showing the ends of the magnet solenoids (d) and the tapered iron cores of tweezers (e) projecting over the custom-built sample dish (f). The dish rests on a heating plate (g) and can be moved with the microscope's sample stage relative to the tweezer tips. **(D)** Schematic of the sample dish, showing the AMPAD sample location, the tweezer tips (gray), the acetal base (blue) and lid (green) of the dish, and the PDMS ring (yellow) that seals the space for culture media (pink). See text and Figure 7 for further details. Panel C is reproduced from (Shi, 2020). Used by permission. Panel D is reproduced from (Shi et al., 2019).

Norpix Streampix software (Version 5.16 or later)  
 Gigabit Ethernet camera (Allied Vision GX1050, or equivalent)  
 Kepco BOP 50-2M power supply.  
 Hall sensors (Lakeshore HGT-2101)  
 Inverted microscope (Nikon TE-2000E or equivalent)  
 10×, NA = 0.3 air objective (Nikon Plan Fluor)  
 40×, NA = 0.6, extra-long working distance air objective with correction collar (Nikon Plan Fluor).  
 100 W halogen illuminator  
 long-working distance condenser with NA = 0.52.  
 Ultraviolet (UV) (Edmund Optics, cat. no. 64-667) and infrared (Edmund Optics, cat. no. 47-303) filters  
 Microscope enclosure incubator (In Vivo Scientific, Inc. Model CH.HC5.SAT, or equivalent)  
 Microscope stage heating plate (20/20 Technologies, Model TC-500, or equivalent)  
 Pipettes (200 and 20  $\mu$ l)  
 Vacuum grease  
 UV cabinet (Model KT-16DC, Foshan Shunde South Electric Appliance, or equivalent)

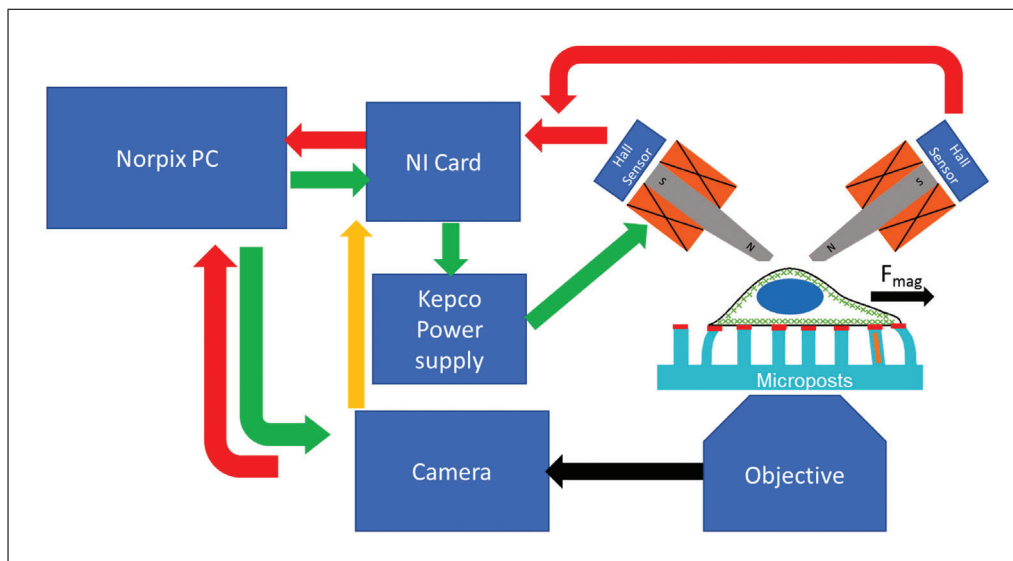


**Figure 6** Block diagram of the measurement system for AC cellular rheology measurements with magnetic microposts. Green arrows: flow of control from PC to camera and magnetic tweezers. Red arrows: flow of image data from camera and magnetic field data from Hall sensors to the PC. Yellow arrow: trigger output from camera to NI card to synchronize the Hall sensor measurements with the image frame capture. Note that the Kepto power supply is operated in current programming mode.

*Further information on the sample dish used for cell rheology measurements: as shown in Figures 5D and 7, a 50-mm culture dish is fabricated out of acetal plastic. A standard square coverslip (22 mm width  $\times$  0.17 mm thick) (shown edge-on in Fig. 5D) is glued with PDMS into a cutout in the dish to allow optical access. A micropost substrate with adhered cells mounted on a similar coverslip fits into the cutout on top of the first coverslip. An acetal lid (green in Fig. 5D) with a beveled top allows the magnetic tweezer tips (gray) to be brought within 1 mm of the cells without contacting the culture media (pink in Fig. 5D). The lid has a coverslip glued into it to allow illumination, and the culture media should fill the volume between the dish and the lid. The lid has four 2-mm posts in a square pattern that fit into corresponding indentions in the dish to prevent motion of the lid. A PDMS ring (orange in Fig. 5D) covers the open area between the edge of the lid and the dish to reduce media evaporation. The PDMS ring may be cast in a suitably sized Petri dish with a cylindrical insert (metal or plastic) to define the inner radius of the ring. The dish, lid, and PDMS ring are shown in Figure 7.*

1. Configure the microscope for white light imaging of the magnetic microposts as described in Basic Protocol 2, steps 8-15.

2. Mount the dual magnetic tweezers onto the microscope. (Fig. 5)

*If the magnetic tweezer tips are rusty, use a grinding wheel or sandpaper to clean them. Then add a drop of PDMS and bake at 70°C overnight. This will protect the tips from oxidation.*

3. Pre-heat the system with the stage incubator to 37°C.

*This will take approximately 4 hr.*

4. Set up the Streampix software as described in Support Protocol 2.

*This includes special-purpose modules to drive the magnetic tweezers.*

5. Use a tweezer to add a drop of autoclaved vacuum grease at each corner of the custom glass-bottom dish. Place a magnetic AMPAD sample seeded with cells onto

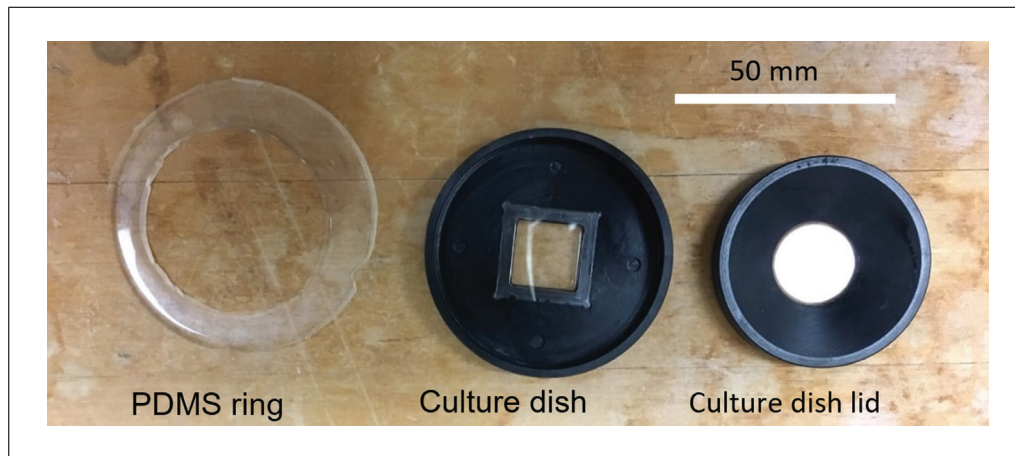


**Figure 7** Components of the custom sample dish for cell rheology measurements. The PDMS ring has an outer radius of 55 mm and an inner radius of 45 mm. Reproduced from Ref. (Shi, 2020). Used by permission.

the glass bottom of the custom-built sample dish (Fig. 7) and ensure firm contact between the glass bottom of the sample dish and AMPAD.

*The grease prevents the AMPAD sample from moving during measurements.*

6. Immediately add 1 ml of CO<sub>2</sub> -independent culture media into the dish and place the custom culture dish lid (Fig. 7) over the sample.

*This must be done quickly to ensure that the cells do not dry out. Make sure that the four posts on the bottom of the lid fit into the holes in the dish.*

7. Seal the sample dish with a PDMS ring.
8. Raise the tips of the magnetic tweezers and slide the sample dish under the tweezer tips.
9. Using the 40× objective, adjust the focus of the microscope until the tops of the posts are in focus, rotate the sample dish so that rows of posts (in the hexagonal grid) are aligned horizontally (see Basic Protocol 2, Section 2.2, step 10), and then raise the focal plane of the microscope by 1 mm above the tops of the posts.
10. Switch to the 4× objective and lower the tweezer tips until they are in focus.
11. Switch to the 10× objective. Adjust the lateral position of the tweezer tips until they are in the middle of the field of view and 500 μm apart.
12. Lower the tweezer tips by 200 μm.

*This can be done by lowering the focal plane by 200 μm and adjusting the tweezer position until the tips are in focus. The goal is to have the tweezer tips just above the top of the indented section of the sample dish.*

13. Switch back to the 40× objective.
14. Switch on the camera in the Norpix software.
15. Find a cell with one or more magnetic microposts underneath it.

*Typically, magnetic microposts look like regular microposts, except they are darker. Normally there will be defects in the MPADs, such as collapsed posts, and they can be used as landmarks to mark the cell's position. If the MPAD arrays do not have fiducial marks, it is best to look for cells near the edges of the arrays. This facilitates finding the cells' locations again in later stages of the protocol when the magnetic posts are re-measured after the cells have been removed.*



16. Optimize the image quality and set the Norpix gain as described in Basic Protocol 2, steps 18-22.
17. Start the Kepco power supply and click on the Record button in Streampix. The software will drive the magnetic tweezer automatically and carry out measurements at a set of frequencies between 0.1 and 135 Hz (0.1, 0.2, 0.5, 0.8, 1, 2, 4, 5, 8, 10, 20, 35, 55, 80, 95, 115, and 135 Hz). The movie taken at each frequency will be saved in a separate AVI file.

*In our system, an AC current of 100 mA peak-to-peak from the Kepco power supply produces a magnetic field of 10 mT, which yields a torque of 1.5 nN• $\mu$ m on a 5- $\mu$ m magnetic nanowire and hence a  $\sim$ 250 pN effective force on the cell adherent to the magnetic post. This low force range minimizes the mechanical stimulation applied to the cells to remain in the regime of linear response. It is important to note that the driving current should not exceed the safe operating limits of the solenoids in the magnetic tweezers to avoid any risk of burning them out. Therefore, the hard current limits on the Kepco BOP should be preset manually following the manufacturer's manual. As the BOP should be operated in current-programming mode, ensure that the inductive voltage across the tweezers does not exceed the voltage compliance of the BOP at the highest frequencies studied.*

18. After finishing recording, shut down the Kepco power supply, move the file(s) with the readout from the Hall sensors into the same folder with the AVI files, and repeat steps 15-17 for additional cells as desired.
19. When finished with data acquisition, raise the tweezer tips and take out the sample dish.
20. Open the lid of the sample dish and rinse the MPAD array with 1 ml of PBS.
21. Add 1 ml of trypsin-EDTA preheated to 37°C into the dish and leave for 5 min to allow the cells to be removed from the microposts. Then pipette out the remaining solution inside the dish and refill with DI water at 37°C.
22. Put the lid back on to the sample dish.
23. Repeat steps 7 to 19 to measure all the fields of view where cells were measured.

*This is intended to measure the magnetic microposts' rheology after removing the cells. In Basic Protocol 5, this will be subtracted from the overall modulus (cell plus post) measured in steps 7-19 to obtain the cell's modulus.*

24. Clean the customized dish with ethanol, then put it in the UV cabinet for 30 min.

*This is to sterilize it for the next use.*

## **CONFIGURING STEAMPPIX FOR MAGNETIC RHEOLOGY MEASUREMENTS**

This support protocol describes the procedures for setting up Streampix to load modules that drive the dual magnetic tweezers with varying frequency magnetic fields, measure Hall voltages from the tweezers, and perform image acquisition simultaneously. It assumes one uses Streampix 5.16 to drive the camera on the microscope and that the user has access to our custom software modules. Once a video file is created, the driving module will run its “Start” command and generate a sinusoidal wave composed of a signal frequency ranging from 0.1 to 135 Hz and a reference frequency at 7 Hz in the output channel of a NI DAQ card. Then, whenever an image frame gets recorded, the module will run its “Increment command,” which will read the magnetic field from the Hall sensor. Finally, when the recording stops, the driving module will run its “Stop” command, which shuts down the NI card's input and output channels. These 3 steps continue iteratively until all frequencies to be measured are covered.

## **SUPPORT PROTOCOL 2**

Shi et al.

---

17 of 47

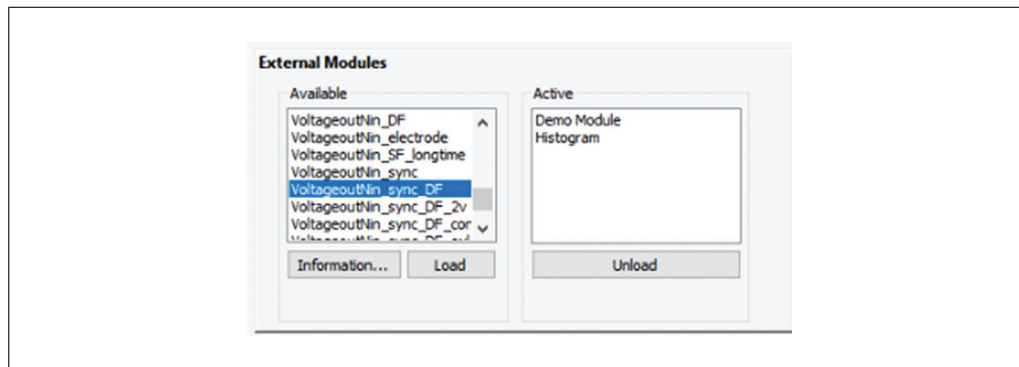


**Figure 8** Screenshot of module list in Streampix. Choose VoltageoutNin\_sync\_DF for active microrheology data acquisition.

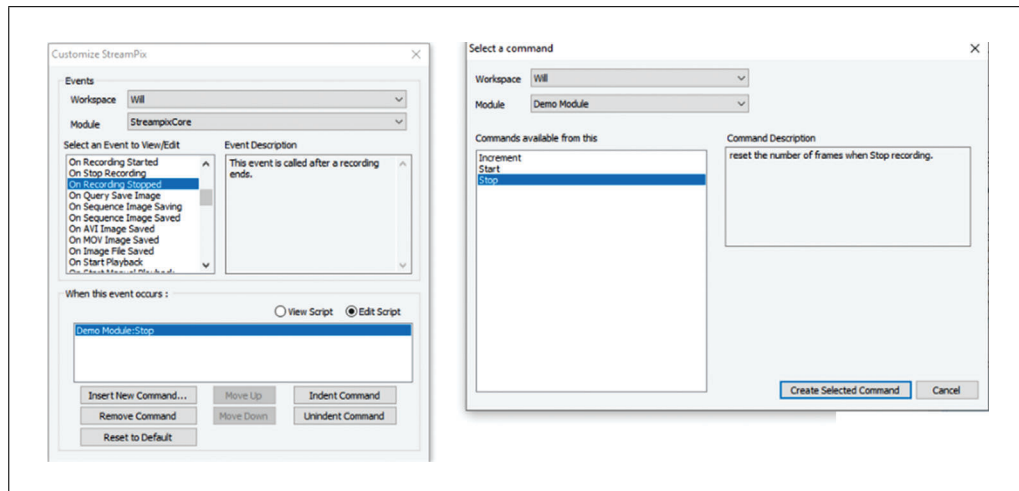


**Figure 9** Screen shot for setting up the command “Start” under the event “On PostCreate AVI.”

1. Open Streampix (the camera driving software), load the module “VoltageoutNin\_sync\_DF” (Fig. 8), then under the Tools panel in Streampix, click “reload saved script”.

*For first time users, under the Tools panel in Streampix, click Edit Script, then under channels, select the module streampixCore; under the event On PostCreate AVI, insert the command “Start” from “Demo Module” to set up channels in the NI card to output a sinusoidal wave and take readout from the Hall sensors (Fig. 9). Under the event “On recording stopped,” insert the command “Stop” to close the two channels mentioned above (Fig. 10). Under the event “On AVI image saved,” insert the command “Increment” (Fig. 11) to record the readout from the Hall sensors each time a frame is captured. Once all these are set, close the editing window, and click “Save Current Scripts” (Fig. 3) so that these settings can be reloaded the next time you run Streampix.*

2. In Streampix Settings, in the Auto Naming panel, check “Auto naming new videos” (Fig. 12). Then under the Recording Rate panel, set it to “Use a recording script” (Fig. 13) and load the script “synchronizedscript”.

*The recording script will iteratively record 17 videos, covering the frequency range from 0.1 to 135 Hz. It will record for 180 s for frequencies under 1 Hz, 60 s for frequencies between 1 and 10 Hz, and 30 s for frequencies between 10 and 135 Hz. It will skip the frames in the first and last 30 s of the video so that any transient response of the magnetic microposts when the driving frequency is changed will have time to damp out.*

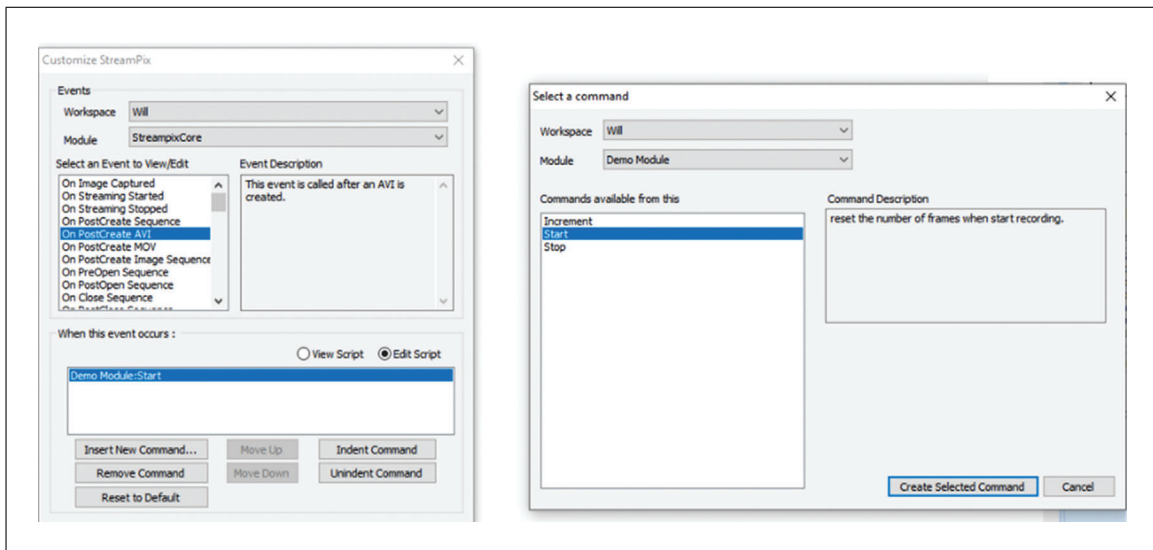


**Figure 10** Screen shot for setting up the command “Stop” under the event “On Recording Stopped.”

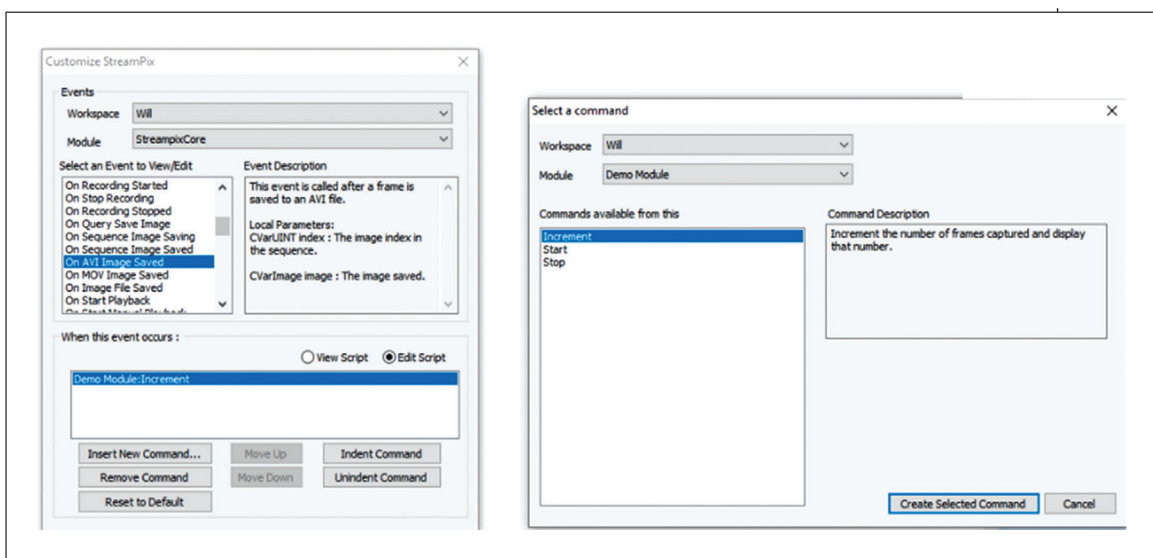


**Figure 11** Screen shot for setting up the command “Increment” under the event “On AVI Image Saved.”

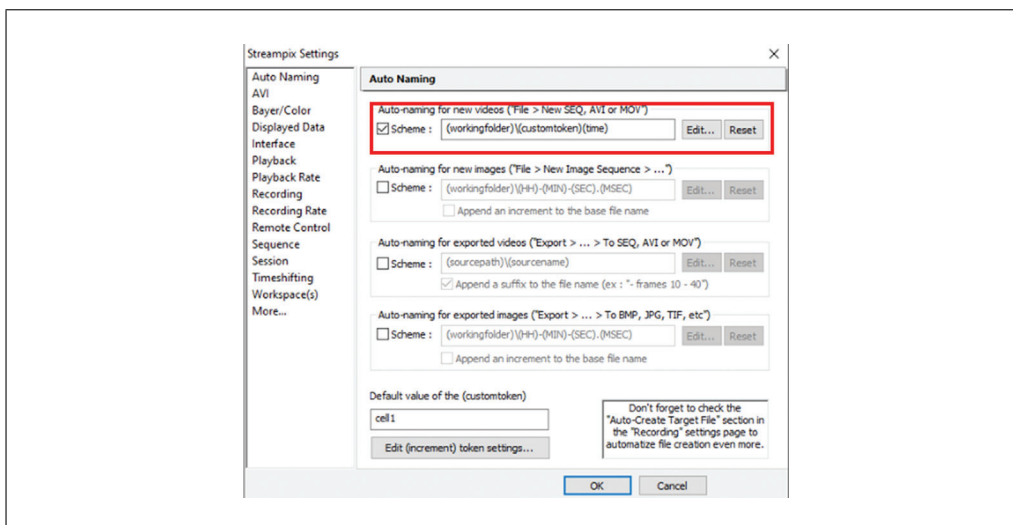


**Figure 12** Screen shot for setting up the auto-naming and file naming convention in the Streampix settings.

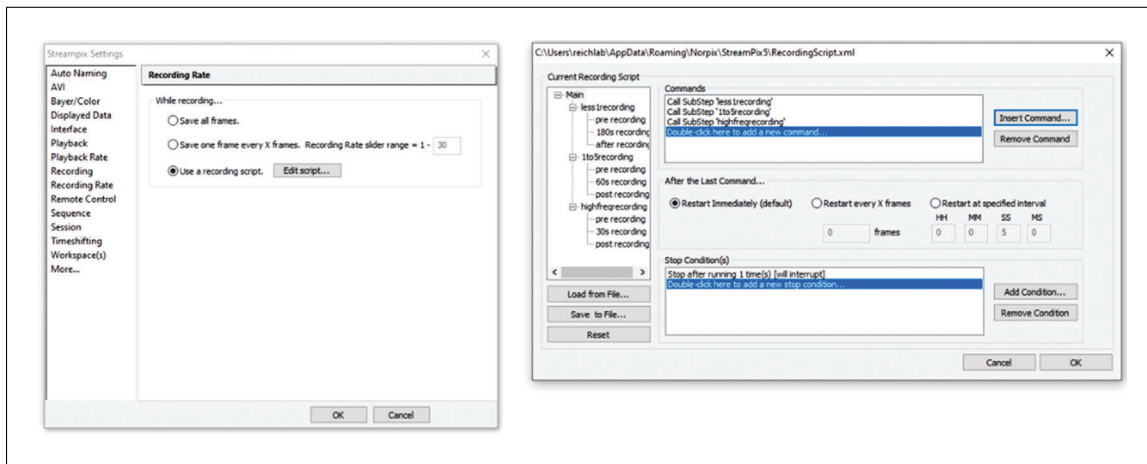


**Figure 13** Screen shot for use of recording script when imaging.

## BASIC PROTOCOL 4

### DATA REDUCTION: DETERMINING MICROPOSTS' MOTION

The data acquisition of either non-magnetic or magnetic measurements results in videos of the microposts' motion at up to 100 fps for each cell measured. This protocol describes a procedure to reduce these raw data to obtain the position of the center of each micropost in each video frame to allow the construction of position versus time traces for each post. This protocol uses a centroid-based particle tracking algorithm (Crocker & Grier, 1996) widely used in the microrheology literature. The custom version used, written in Igor Pro, takes advantage of the known underlying lattice of the posts. One begins by using a visual inspection of the first frame of the movie to define an initial mask that classifies the posts as either "cell posts" that are in contact with the cell, "background" posts that are not in contact with the cell, or "ignored" posts. The ignored posts are not analyzed and should include broken or bent posts and posts that may be under cells in the field of view other than the one to be analyzed. The distinction between cell posts and background posts is initially provisional and will be refined in subsequent stages of the analysis. Frame-to-frame drift is accounted for by measuring the average displacement in each frame relative to the first frame for all the background posts and subtracting this from each post's trajectory. To avoid including cell posts in the dedrifting calculation, it is thus better to err initially on the side of classifying posts near the cell as cell posts rather than as background. The undeflected positions of the cell posts are then determined by interpolation based on the positions of the background posts in corresponding rows and columns of the post lattice. The undeflected positions are subtracted from the raw positions to yield the posts' deflections versus time for subsequent analysis. Note that long movies at high frame rates can be time-consuming to process.

#### Materials

PC or Macintosh computer (e.g., Dell Precision Tower 5810)  
 Igor Pro Software (Wavemetrics, Inc, version 8 or higher)  
 Custom Igor Procedure Files (See Internet Resources)

1. Launch Igor Pro, load the procedure file Centroid\_Fit\_Main\_V11.ipf, and compile it.

*This will load several other Igor Pro .ipf procedure files via #include statements. These #include statements will have to be modified to work on each user's computer.*

2. Run the function GfitGridAllM() from the Igor Pro command line to open the main graphical user interface (GUI) (Fig. 14)

*This GUI controls all the data reduction and analysis functions described in this paper.*

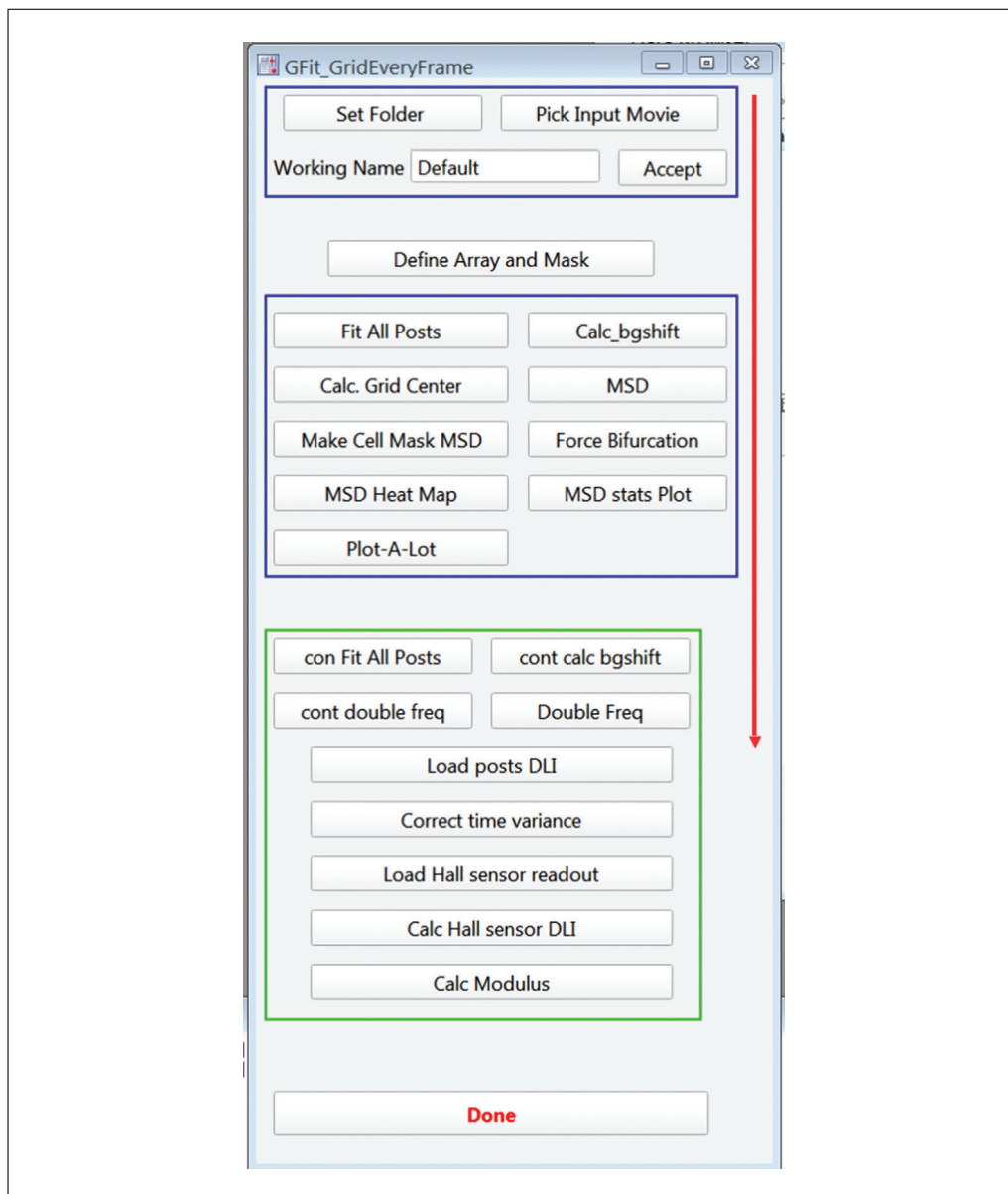


**Figure 14** Main Igor Pro graphical user interface (GUI) for data reduction and analysis.

3. Click the “Set Folder” button and choose the folder where the data video file to be analyzed is stored.
4. Click “Pick Input Movie” and load the video file to be analyzed. You may have to set the Data Files file type to “all files.”
5. In the “Working Name” field, enter a new folder name. This will create a folder with the name you enter, and results from all following analyses will be stored there. Click Accept.

*This name should be similar to the input video file’s name to simplify record keeping.*

6. Click the “Define Array and Mask” button to open the GUI (Fig. 15) for defining the set of microposts to be analyzed and setting up the initial mask classifying the posts as cell-associated, background, or ignored for subsequent analysis.
7. Click Initialize, Pick ROI, and enter “0” in the pop-up panel (Fig. 16) to start a new analysis. Click Continue.

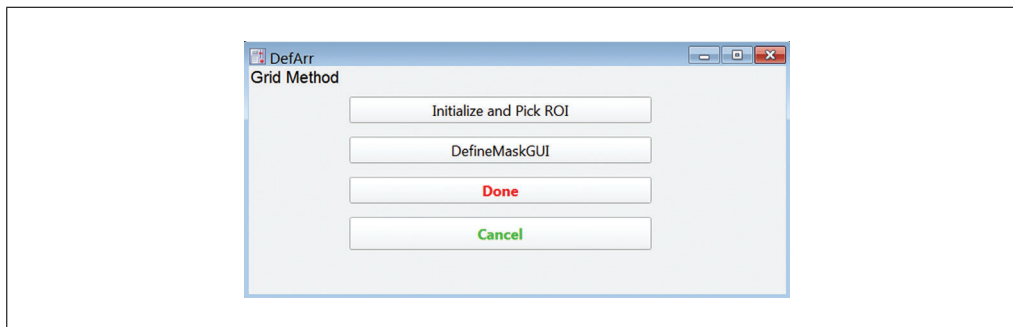


**Figure 15** GUI accessed from “Define Array and Mask” in main GUI. It is used to define the set of posts to be analyzed and provide an initial mask classifying the posts.

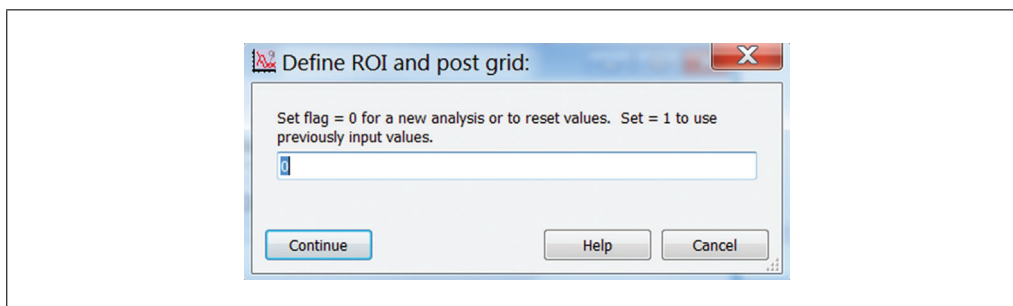


**Figure 16** Input window in Initialize and Pick ROI to reset ROI or use previous settings.

*Enter “1” if you are re-running a previous analysis. This will recall the positions of your ROI boundaries, but you will have to rotate the image again.*

8. The Input Parameters GUI (Fig. 17A) and an image of the movie’s first frame should now be open. Rotate the image (positive for clockwise) so that the horizontal axis of the hexagonal grid of posts aligns with the horizontal axis of the image frame by entering an angle in the “Angle (degrees)” box and clicking Rotate to carry out the rotation.

*This is an incremental rotation from the current image orientation. Successive image rotations can be carried out as needed. Use the Revert button to return to the original unrotated orientation. The rows of posts do not have to be exactly horizontal but should be within  $\pm 0.1$ – $0.2$  degrees of horizontal. The rotation operation may have uncontrolled effects on image quality. It is important to have the post arrays lined up close to horizontal when the data are acquired in Basic Protocols 2 and 3.*

9. Define the region of interest (ROI) around the target cell to be analyzed. This is a two-step process. First, draw a rectangle to roughly define your ROI. Click Draw Rectangular ROI. Click Draw Mode in the upper left of the image frame, select the Rectangle tool and draw a rectangle to define the ROI containing the cell you wish to analyze. Center the upper left corner of this rectangle on a micropost.

*This is an initial step, and the ROI bounds will be refined further in step 11. It is best to get the rectangle’s upper left corner close to the center of a post. Get the upper right corner close to a post as well (it may not be exactly on a post if your rotation correction is not perfect), and position the lower-left corner close to the row of posts that you want to be the bottom of your ROI. If it is necessary to adjust the position and shape of the rectangle after it is drawn, click on the Arrow (selector tool) in the Igor drawing menu, click on the rectangle and adjust as needed.*

*Important: Do not try to analyze posts right up to the boundary of the image. Leave at least a one-post gap between the ROI and the edge of the frame. Reducing the ROI size to avoid analyzing too many background posts can speed up the analysis. However, it is very important to leave a border 2-3 posts wide at a minimum around the cell in all directions. This border of background posts will be used to define a grid to determine the*

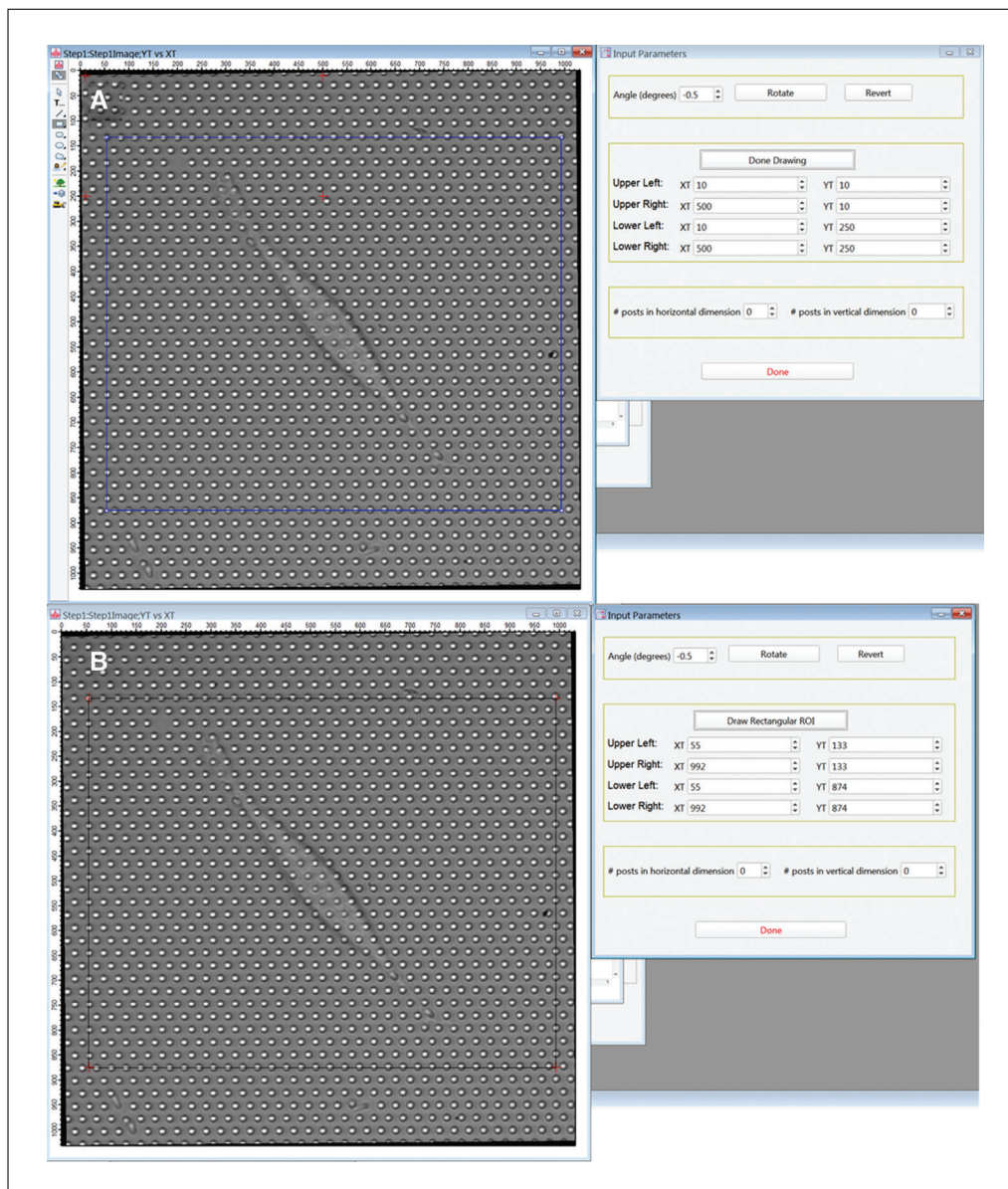


**Figure 17** (A) GUI for setting the ROI centered on the cell to be analyzed and containing the posts to be tracked. After rotating the image so the rows of posts are horizontal, the drawing tools (upper left) are used to define a rectangular ROI. (B) After clicking “Done Drawing,” the positions of the four corners are updated in the GUI and are marked by the red crosses in the image.

*undeflected positions of the posts in contact with the cell. This is needed to measure the absolute post deflections and hence the absolute values of the cellular traction forces.*

10. Click Done Drawing in the GUI. The positions of the corners of the rectangle you drew should appear in the boxes labeled XT and YT, and the red crosses in the image will move to the corners of the rectangle in the image (Fig. 17B).

*The positions of red crosses are what the program uses to define the post lattice and ROI, so these now need to be refined.*

11. Adjust the positions of the red crosses using the up- and down-arrows by the x- and y-position values in the GUI to center them on posts. All the crosses should end up within 2 pixels of a post center. First, if necessary, adjust the upper left red cross.
12. Next, adjust the position of the upper right red cross to center it on a post in the same row as the upper left cross. Count the number of posts between the two upper

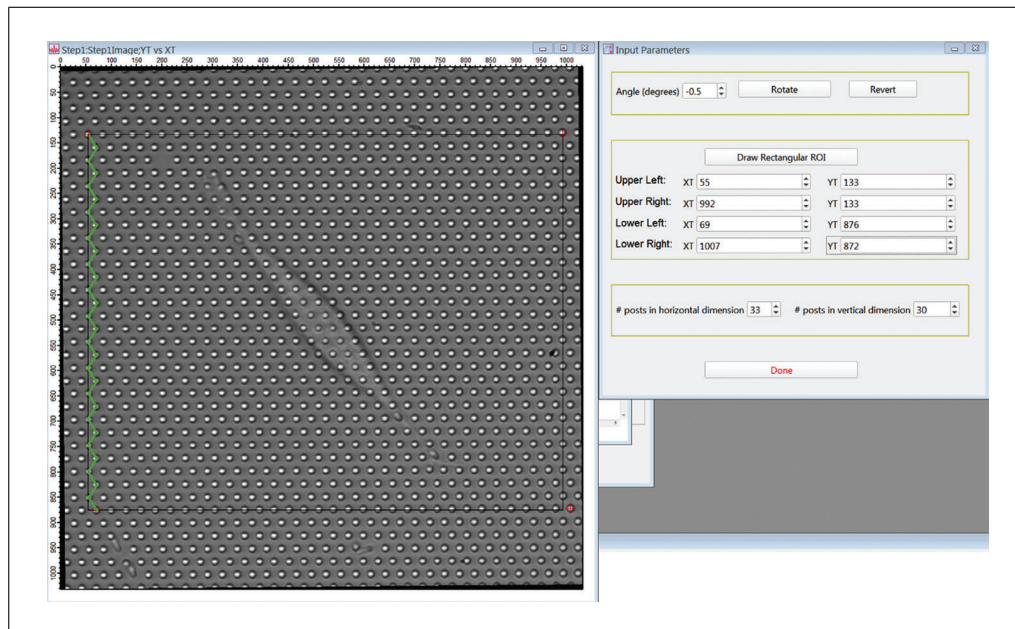


**Figure 18** Illustration of adjustment of the two crosses at the bottom of the ROI to move them on top of the microposts. The green line indicates the path along which to count the posts in the vertical direction.

crosses, including the posts under both crosses, and enter this number in the “# posts in horizontal dimension” box.

*Each corner of this rectangle must be closely centered on a micropost (within 2 pixels). If it is necessary to adjust the position and shape of the rectangle after it is drawn, click on the Arrow (selector tool) in the Igor drawing menu, click on the rectangle and adjust as needed.*

- Now position the lower-left cross. Count from row to row down the image from the upper left cross following a zig-zag path like the one shown in green in Figure 18. Enter the number of rows in the “# posts in vertical dimension” box. Again, include both the starting and ending rows in your count.

*Your counting path may deviate from the boundary of the rectangle drawn in step 9 if the rotational alignment is not perfect or if the array (or the image) is in some way distorted. If you have an odd number of posts in the vertical dimension, the lower-left red cross should be directly under the upper left cross if the post lattice is perfectly aligned. If you have an even number of posts in the vertical direction, the lower-left cross will be one-half of a lattice constant to the right of the upper-left cross.*

- Finally, position the lower-right cross. This can be done either by counting horizontally from the lower-left cross or vertically from the upper-right cross.

*Figure 18 provides an example of the results of this procedure.*

- Press Done when finished.
- Click the “DefineMaskGUI” button to open the SetMaskPanel GUI for defining post types. Enter 0 in the popup window (not shown) to use the first frame in the movie to set the mask.

*It can occasionally be useful to use a different frame if one wants to start analysis at some later point in the movie.*

- Click Continue. In the first frame image, a red cross should appear over each post in your RO (Fig. 19). This is the default identifier for a background post. The locations of these crosses will be used as the initial guesses for the positions of the centroids of



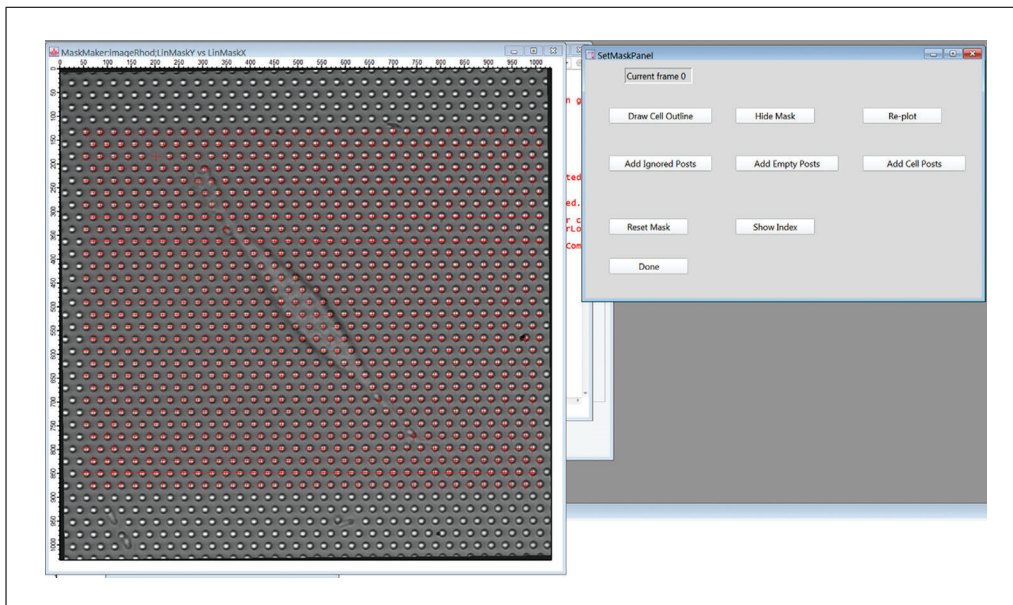


**Figure 19** GUI for SetMaskPanel to create the initial identification of cell-associated and background posts, and defective or other posts to be ignored in the analysis. All posts are initially labeled as background posts (red crosses).

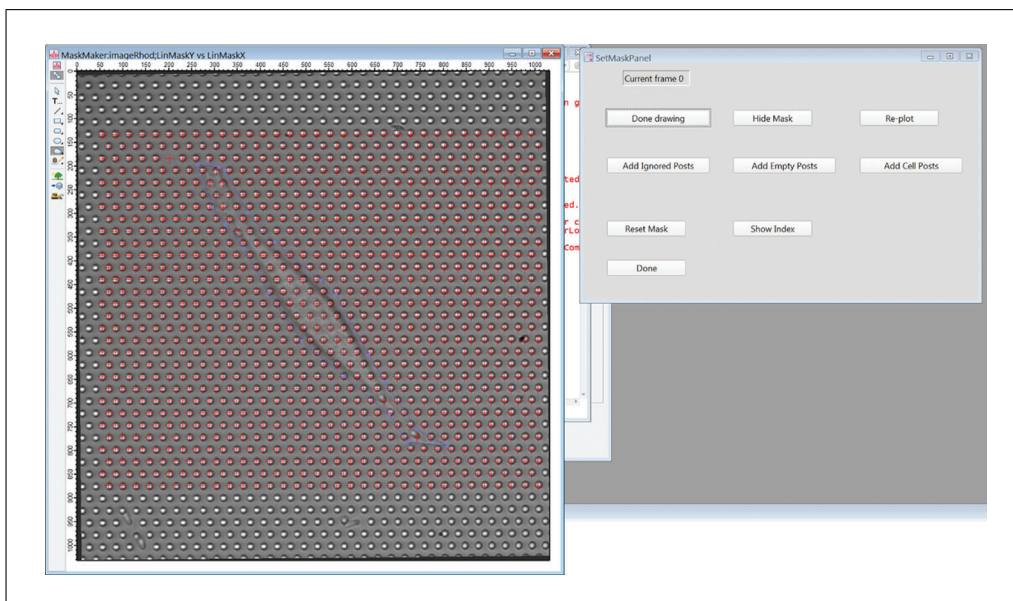


**Figure 20** Drawing panel to manually draw the cell outline with the IgorPro polygon tool.

the posts when fitting the first frame. If the crosses are not well reasonably lined up with the posts, you will have to go back to Step 6 and re-define the ROI and numbers of posts.

*Check that you counted the right number of posts in each direction. If you have miscounted, the crosses in the middle of the image will be systematically out of registry with the posts.*

18. Identify the cell-associated posts (“cell posts”) by clicking the “Draw Cell Outline” button. Click on the Draw Mode button in the upper left of the image frame, select the Polygon tool and draw a polygon enclosing the cell (Fig. 20). When finished, click the “Done Drawing” button, and then in the pop-up window, enter 1 to identify all posts inside the polygon as cell posts. Click Continue.

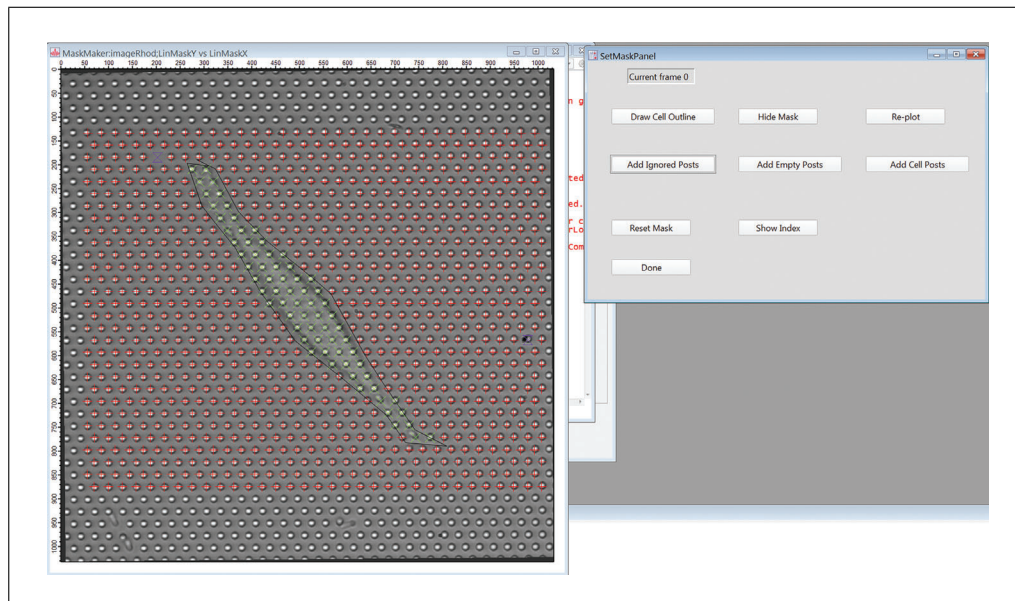


**Figure 21** View of mask array showing background posts (red crosses), cell posts (Green x) and ignored posts (purple hourglass symbols).

*All posts in the polygon should now be marked with green x's identifying them as cell posts. (Fig. 21)*

19. Click “Add Ignored Posts”, then click on any posts in the image frame that you do not want to analyze. This should include any posts that are missing or collapsed, plus any posts that are under cells other than the cell to be analyzed. When finished, click on the “Done Adding” button.

*All ignored posts will be marked with purple hour-glass symbols (Fig. 21).*

20. Adjust the mask further as needed using the “Add Cell Posts”, “Add Empty Posts”, and “Add Ignored Posts” buttons, followed by clicking on the image frame to change posts to cell, background (empty), and ignored respectively. Click “Done Adding” after working with each post type.

*As noted in the introduction to this protocol, since the background posts are used to do the frame-to-frame dedrifting correction, to avoid including cell posts in this calculation, it is better to err initially on the side of classifying posts near the cell as cell posts, rather than as background.*

*Note that there are other buttons in this GUI that can be helpful here and at various stages in the analysis. “Hide Mask”, “Replot”, and “Reset Mask” carry out the corresponding operations on the mask. “Show Index” replaces the mask symbols with the index of each post in the various data storage arrays.*

21. Click “Done” in the “SetMaskPanel” GUI (Fig. 21) and in the “DefArr” GUI (Fig. 15) to finish defining the mask.

*The locations of the points in the mask will be used as initial guesses for the post positions in the analysis of the post trajectories.*

22. Click “Fit All Posts” in the main GUI (Fig. 14) to start centroid fitting of all the posts’ trajectories. In the pop-up window, enter the number of the first and last frames to be analyzed (Fig. 22). You can choose whether to have an image of each frame shown as it is analyzed. (Use this for diagnostic purposes only, as this will be slower). You can also have the current frame number printed periodically to track progress as the analysis runs. The fit post centers will be stored in units of pixels in the 3D wave

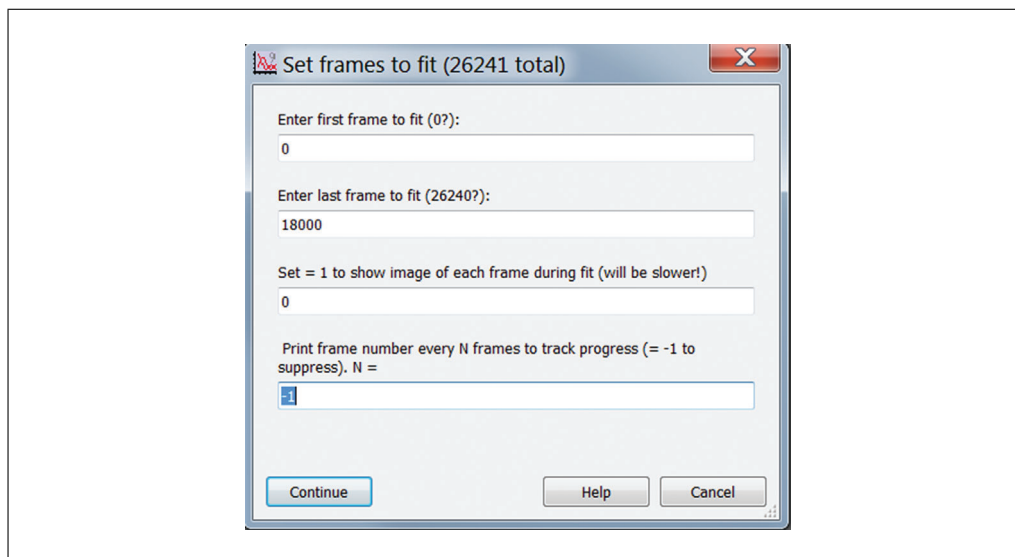


**Figure 22** Pop-up window for “Fit All Posts” button.

FitRes\_XXX, where “XXX” is the string entered in the Working Name field. The Layer dimension is the frame number.

*When running this initially, it can be useful to analyze only the first few frames of a video to verify that the process is working and to estimate the run time before attempting to analyze a long movie.*

*For a 10-fps video of 30 min duration (18,000 frames), this step will take approximately 30 min on a Dell Precision Tower 5810 PC.*

23. Click the “Calc\_bgshift” button in the main GUI (Fig. 14) to correct for frame-to-frame background drift. For the initial analysis, choose “manual” in the pop-up window.

*“Manual” will use the post identification mask defined in steps 16-21. If desired, this can be refined after MSD analysis using “automatic” mode, which uses the more accurate MSD-based identification of cell and background posts. This can be used to correct issues that may arise with the dedrifting computation if cell posts are erroneously identified as background posts in the manually created mask. The automatic mode can only be run after the Make Cell Mask and Force Bifurcation operations are run, as it uses the mask wave generated in the latter procedure (See Basic Protocol 6.). In this case, repeat Step 24 below and run through the analyses in Basic Protocol 6 again.*

24. Click the “Calc Grid Center” button in the main GUI (Fig. 14) to calculate the undeflected positions of the posts. In the pop-up window, enter the same number of frames analyzed in Fit All Posts in step 22.
25. As desired, use the “Plot-A-Lot” button to view the trajectories of the posts. The popup window for this function is shown in Figure 23. You must use Manual in the Mask Type dropdown menu at this stage of the analysis.

*PlotALot will show the x- and y- components of the posts’ trajectories. Examples of such plots are shown in Figures 33-35 and are discussed in the Commentary below. Set “Y” in the “Print in Right Column” dropdown menu. If you are looking at more than 7 posts, set the notebook flag to 1 (the default) to output the plots in an Igor notebook. Use the “Trajectory to plot” dropdown menu to view the raw trajectories, the dedrifted trajectories (after Calc\_bkshift is run), or the displacements of the posts from their undeflected positions (after Calc.Grid Center is run). The traces are colored black for background posts (post type 0), green for cell posts (post type 1), and gray for ignored posts (post type 3). The plot legends also give each post’s index in the FltRes\_XXX wave and its position (a,b) in the 2D mask waves, where a is the position in a row of the hexagonal lattice, and*

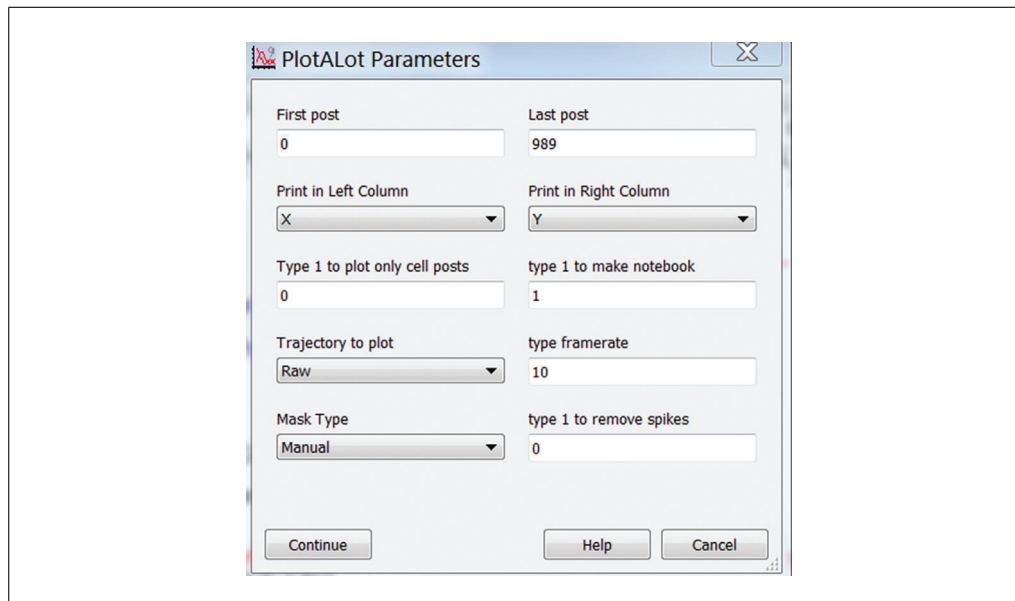


**Figure 23** Pop-up window for “Plot A Lot” button to display displacement traces versus time.

*b* counts vertically down the rows in a zig-zag manner. Posts can be identified by number by going to Define Array and Mask > DefineMaskGUI>ShowIndex.

**BASIC  
PROTOCOL 5**

**DATA ANALYSIS: DETERMINING LOCAL RHEOLOGY FROM MAGNETIC MICROPOSTS**

This protocol extracts the frequency dependence of the cellular rheology from the motion of the magnetic microposts in response to AC magnetic fields. The centroid-based particle tracking algorithm (Crocker & Grier, 1996) used in Basic Protocol 4 is used again, but the software is modified to handle the sequence of recordings at different magnetic field frequencies generated in Basic Protocol 3. Then digital lock-in analysis is applied to extract the response of each post at the (variable) drive frequency  $f$  and the reference frequency  $f_R$ . Magnetic posts are identified by their large response compared to non-magnetic background posts. To account for time-dependence in the amplitude of the response at the drive frequency, the signals are broken up into 10 s intervals, and the average of the ratios of the displacements  $x(f)/x(f_R)$  are computed (see Commentary). The driving force is deduced from the magnitude of the magnetic fields and used to calculate the modulus  $k(\omega)$ . As this is the combined response of the cell plus the post itself,  $k(\omega)$  is also computed for data obtained after removing the cells (see Basic Protocol 3), and then the two results are subtracted to obtain  $k(\omega)$  for the cell alone.

**Materials**

- PC or Macintosh computer (e.g., Dell Precision Tower 5810).
- Igor Pro Software (Wavemetrics, version 8 or higher)
- Custom Igor Procedure Files (See Internet Resources)

1. Follow steps 1 to 21 in Basic Protocol 4 to define the analysis ROI, post types, and initial guesses for the post positions.

*The “working name” must be the same as the file root of the movie files. If, for example, filenames are TLBRc2\_1.avi, TLBRc2\_2.avi..., the working name must be TLBRc2.*

*Magnetic posts are not identified separately in these initial steps. They should be classified initially as cell posts.*

2. Click “con fitAllPosts” to track the trajectories of all microposts at each of the 17 frequencies measured in Protocol 3 (Fig. 24). As in Basic Protocol 4, you can

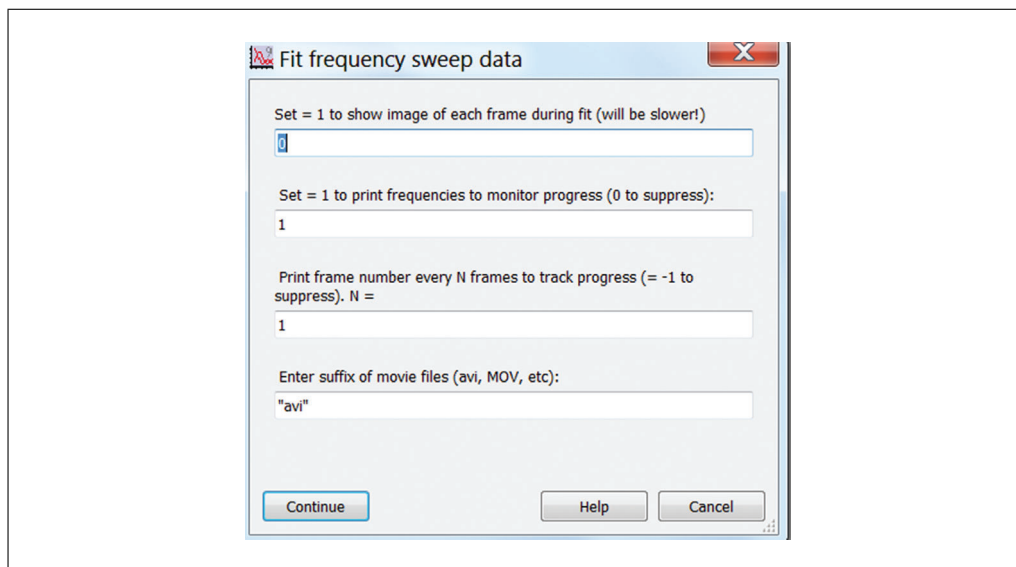


**Figure 24** Pop-up window for “Cont fitAllPosts” to determine post displacements versus time for magnetic rheology measurements.

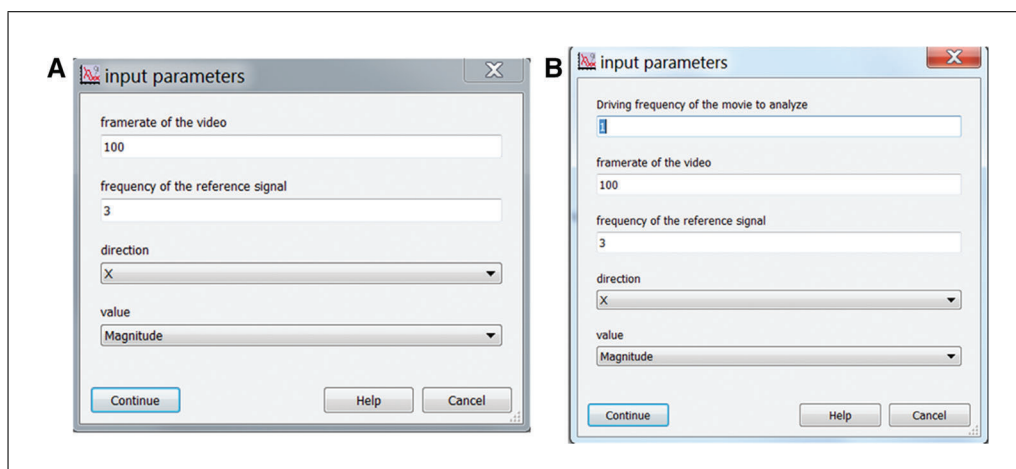


**Figure 25** Panels for calculating oscillation amplitudes via digital lock-in (DLI) from the posts’ deflections. (A) Pop up window when for button “cont double freq” to calculate DLI on all movies taken with different driving frequencies. (B) Pop up window for button “Double freq” to calculate DLI on a specific movie.

choose whether to have an image of each frame shown as it is analyzed in the pop-up window; however, this will be slow, so use this for diagnostic purposes only. You can also choose to have the measuring frequency and current frame number printed periodically to track progress as the analysis runs. The fit post centers will be stored in units of pixels in the 3D wave FitRes\_XXX\_Nhz, where “XXX” is the string entered in the Working Name field and “N” is the frequency. The Layer dimension is the frame number.

3. Click “cont calc bgshift” to perform the background drift correction.
4. Click “cont double frequency” to perform the digital lock-in (DLI) calculation.

*To measure the deflection magnitude in the magnetic field in the X direction, select “Magnitude” in “Value” and “X” in “direction” (Fig. 25A), and enter the proper reference frequency (7 Hz by default). DLI results for movies acquired at all 17 frequencies will be computed, and a heatmap of the DLI results at 0.1 Hz will be generated (Fig. 26), with the color indicating the magnitude of each post’s deflection amplitude at that frequency. To examine the DLI results for a movie taken with a specific frequency, use the “Double*

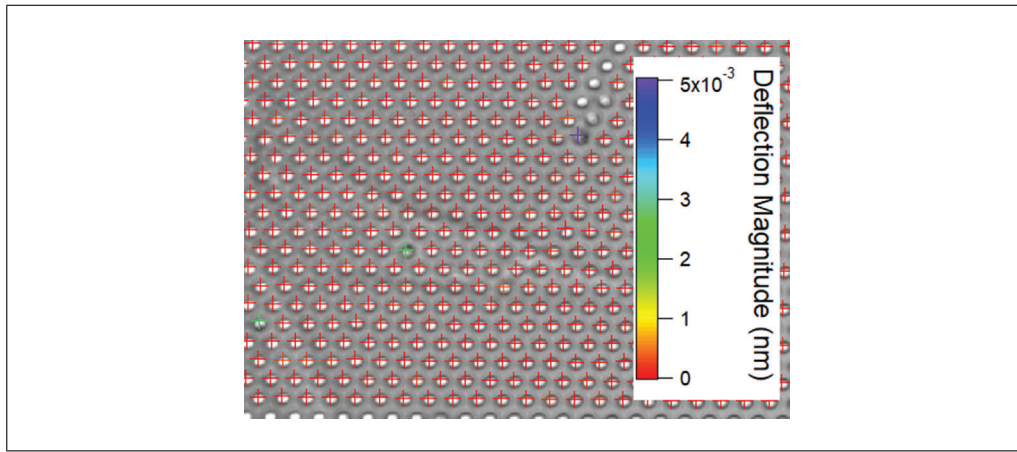


**Figure 26** Heatmap of digital lock-in magnitude at  $f = 0.1$  Hz. The color scale shows the deflection magnitude in nm.

*freq*” button (Fig. 25B). This will require additional input for the driving frequency at which the movie was taken, and a DLI heatmap will be generated.

5. Confirm that the magnetic posts are present by checking the deflection magnitude from the Digital Lock-in result. Normally, deflections of magnetic posts will be larger than 1 nm, whereas the magnitude from a non-magnetic post is  $\sim 0.1$  nm.
6. Click “Load posts DLI” to load all digital lock-in results.

*If needed, navigate to the FILEROOT folder that holds all the results.*

7. Click “Correct time variance” to calculate the frequency dependence of deflection magnitude after correcting for temporal variation based on reference frequency (Fig. 5.4).
8. Click “Load Hall sensor readout” to load all readouts from the hall sensor.
9. Click “Calc Hall sensor DLI” to perform a digital lock-in calculation on the magnetic field.
10. Click “Calc Modulus” to calculate  $k(\omega)$  for all detected magnetic posts.

*In the “Calc Modulus” output, there will be plots of loss modulus, storage modulus, and modulus magnitude versus frequency for different microposts. When double-clicking on figures in Igor, the trace name will indicate the post number for each trajectory, which is correlated with the heatmap generated in Step 4. “Calc Modulus” will also generate a 3D wave called “modulus\_w”, with different columns corresponding to the post number and rows corresponding to the measured frequencies. The first layer stores magnitude of the modulus and the second layer stores the phase. The third and fourth layers are the storage and loss modulus, respectively.*

11. Follow steps 1-11 to calculate  $k_{\text{post}}(\omega)$  for all detected magnetic posts after cells are removed.
12. Open up the two Igor projects in the same field of view with and without cells attached. Calculate the difference  $k_{\text{cell}}(\omega) = k(\omega) - k_{\text{post}}(\omega)$  (Equation 1) by subtracting the frequency dependence of modulus magnitude (data in the first layer of the modulus\_w wave) of the same post in the two projects.

*Usually, the field of view will be slightly different when measuring the modulus with or without cells. Therefore, the post numbers for magnetic posts in  $k_{\text{cell}}(\omega)$  and  $k_{\text{post}}(\omega)$  might differ. View the DLI heatmap in step 4 to find the magnetic posts in the two fields of view.*

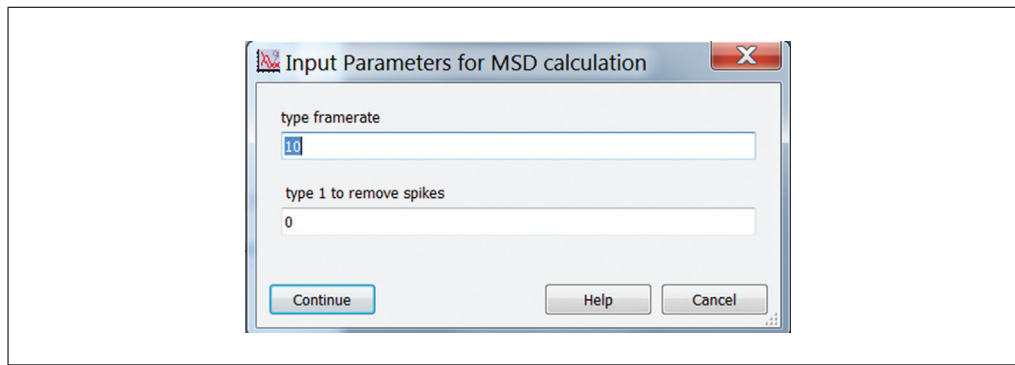


**Figure 27** Pop-up window for mean squared displacement (MSD) calculation.

## DATA ANALYSIS FOR FORCE FLUCTUATION MEASUREMENTS

Measurements with non-magnetic microposts result in time traces that record the mechanical fluctuations of the cell. These are conveniently characterized using the mean squared displacement (MSD)  $\langle \Delta r^2(\tau) \rangle = \langle (\mathbf{r}(t+\tau) - \mathbf{r}(t))^2 \rangle$  (Equation 2), where  $\tau$  is the lag time. The MSD typically shows a power-law dependence  $\text{MSD} \sim \tau^\alpha$  over a range of lag times from roughly 1 to 100 s. A procedure is described to extract the MSD exponent  $\alpha$  by first subtracting the background noise floor and then fitting the logarithmic time derivative of the resultant subtracted MSD. The MSD exponent can then be used for multiple forms of analysis. Background posts that are not connected to a cell typically show much smaller MSD exponents  $\alpha$  than do posts that are connected to a cell, and so the criterion  $\alpha < 0.2$  provides a means to identify the background posts. For long measurement times (e.g., up to half an hour), cell motility can lead to microposts near the edge of the cell being connected to the cell only over a part of the measurement interval as the cell moves. To identify such posts, the MSD may be calculated for the first and last thirds of each time trace, and the requirement that the corresponding exponents  $\alpha_1$  and  $\alpha_3$  both be  $> 0.5$  can be used to identify posts that are connected to the cell throughout the measurement interval. Only these posts are used in subsequent analysis (unless one is interested in tracking motility). Procedures are described to bifurcate the population of cell posts into subpopulations associated with stress fibers and those associated with the cortex based on the average traction force produced on the posts.

### Materials

Igor Pro Software (Wavemetrics, Inc, version 8 or higher)  
 PC or Macintosh computer (e.g., Dell Precision Tower 5810)  
 Custom Igor Procedure files (See Internet Resources)

1. In the main GUI panel (Fig. 14), click the “MSD” button to open a pop-up window for calculating the MSD. (Fig. 27). Enter the video framerate (In frames/s). Set the spike removal flag to 0 initially. Click “Continue”. This will calculate the MSD for the x-component of the motion only. The y-component is not analyzed. The MSD is calculated in units of  $\text{nm}^2$ .

*This may take several minutes to run for long videos. You must have a minimum of 500 frames for the MSD calculation to run. Spike removal deals with some aspects of noisy data by running a sliding window through the data set and detecting outliers using the standard deviation of the points in the window. If the point difference from this sliding mean is 3 times larger than the standard deviation of the points in the 10 nearest frames (before and after), that point is smoothed by averaging.*

2. As desired, the MSD results can be surveyed using “Plot-A-Lot”. Choose “MSD” in the Print in Right Column dropdown menu.

*See Basic Protocol 4, step 25 for further details on Plot-A-Lot.*

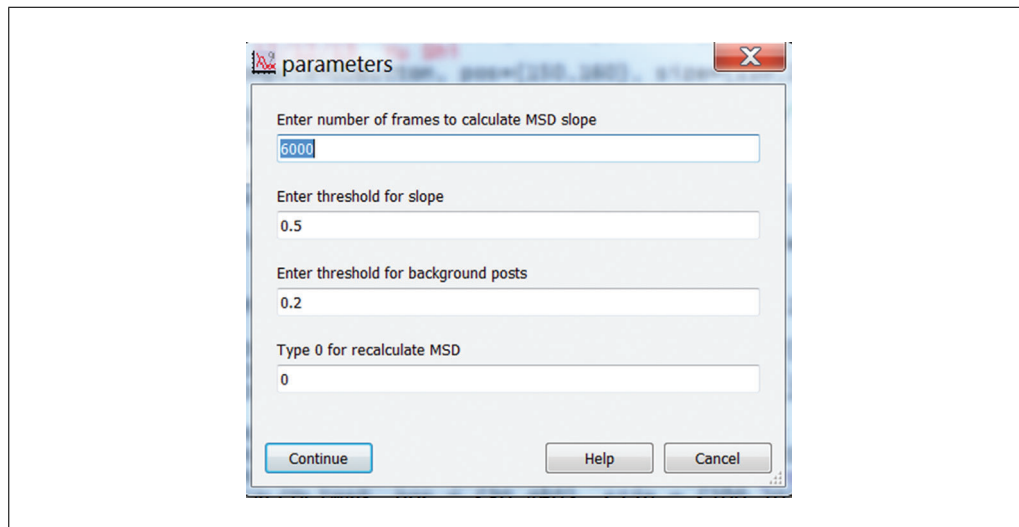


**Figure 28** Pop-up window for “Make Cell Mask MSD” button.

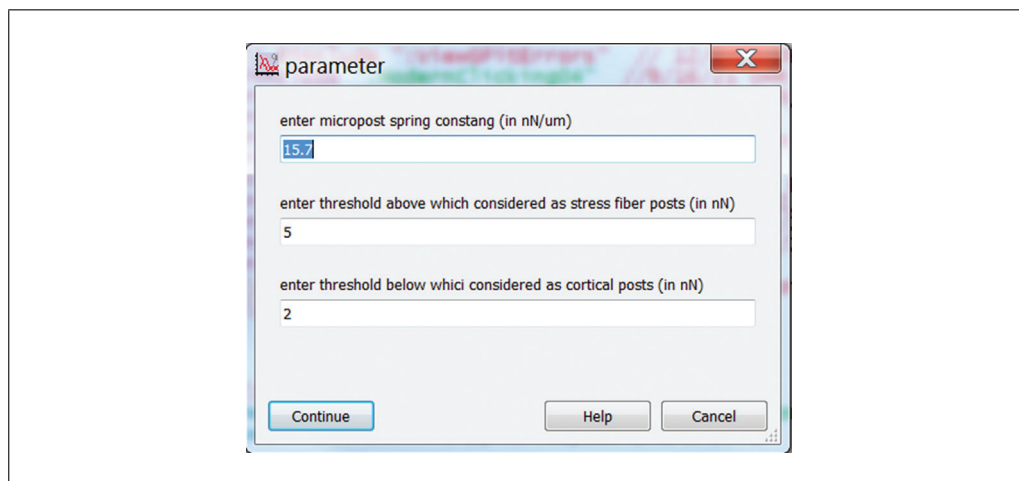


**Figure 29** Pop-up window for “Force Bifurcation” button.

3. When finished with the MSD analysis, click “Make Cell Mask MSD” in the main panel to identify posts associated with the cell based on the MSD exponent. (Fig. 28).

*We normally use 1/3 of the entire video length to calculate the MSD exponent. For a 30-min video at 10 fps, the total frame number will be 18,000, and 1/3 of that is 6000 frames. In “Enter threshold for slope”, normally, one can use 0.5 to make sure all posts categorized as cell posts are associated with the cell. Use 0.2 as the threshold below which posts are identified as background posts.*

4. Click the “Force Bifurcation” button in the main panel and enter post stiffness (in nN/μm) and thresholds for identifying stress fiber and cortical-associated posts to run the code that identifies posts associated with the actomyosin cortex or with stress fibers (Fig. 29).
5. Click the “MSD Heat Map” button; this will generate panels C-E as in Figure 30, which are the heatmaps for the MSD exponent, the MSD magnitude at  $\tau = 10$  s, and the traction force map, respectively.
6. Click the “MSD Scatter Plot” button; this will generate panels F and G in Figure 30, which show the scatter plot of the MSD magnitude at  $\tau = 10$  s against MSD exponent and traction force magnitude, respectively.



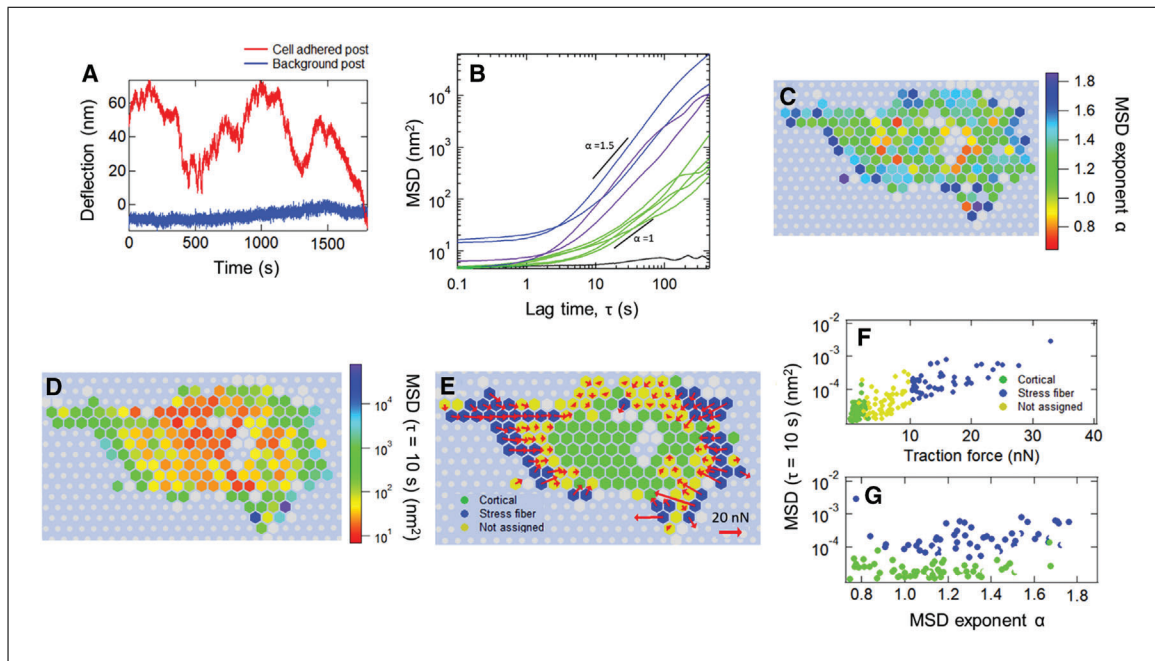


**Figure 30** Sample micropost deflection fluctuations for a cardiac myofibroblast (Shi et al., 2021). **(A)** Deflection trace of one Cartesian component of the motion of a cell-associated micropost (red) and a background micropost (blue) over 30 min (Basic Protocol 4). **(B)** MSDs versus lag time  $\tau$  determined from traces such as those in (A) for the posts indicated by red circles in C. The traces' color shows the MSD power law exponent  $\alpha$  over the range  $5 \text{ s} \leq \tau \leq 10 \text{ s}$  as given by the scale in panel C. The black trace is for the background post shown in A. **(C and D)** Heat maps of **(C)** distribution the exponent  $\alpha$  over  $5 \text{ s} \leq \tau \leq 10 \text{ s}$ , and **(D)** the MSD magnitude at  $\tau = 10 \text{ s}$  Each hexagon represents a post. Gray hexagons indicate posts that were not coupled with the cell over the full measurement interval. Gray circles show background posts. **(E)** Distribution of cortical and stress fiber posts across the cell, as determined by the classification procedure based on average traction force magnitude described in Basic Protocol 6, and the corresponding traction force vectors (red arrows). **(F)** Scatter plot of MSD magnitude at  $\tau = 10 \text{ s}$  versus average traction force. **(G)** MSD magnitude at  $\tau = 10 \text{ s}$  versus MSD exponent  $\alpha$  for cortical and stress fiber posts.

## COMMENTARY

### Background Information

Thanks to the development of microfabrication techniques and the ability to engineer the mechanical properties of substrate materials for cell culture, a variety of approaches have been developed to probe mechanotransduction in cells at various scales (Martino, Perestrelo, Vinarsky, Pagliari, & Forte, 2018; Mohammed et al., 2019). PDMS micropost array detectors (MPADs) are one of the important techniques that have been applied to measure cellular traction forces (du Roure et al., 2005; Geng & Wang, 2016; Tan et al., 2003; Wolfenson et al., 2016). By coating the microposts' tips with fibronectin or other suitable ECM proteins via microprinting, one can achieve controlled coupling between the posts' tips and the cytoskeleton via cellular focal adhesions. For small deflections, the deformation of the microposts in response to cellular traction forces can be modeled by beam bending theory, which provides a method to directly transform the microposts

deflections from their resting positions into the cellular traction force field (Fu et al., 2010; Tan et al., 2003). Further, embedding magnetic nanowires into the microposts provides an approach to applying mechanical perturbations to cells through these same focal adhesion linkages by magnetic actuation (Shi et al., 2019; Sniadecki et al., 2007; Sniadecki, Lamb, Liu, Chen, & Reich, 2008). Another widely used technique to probe cellular traction force is traction force microscopy (TFM), which employs flat substrates with embedded microbead tracers (Plotnikov et al., 2014). The cellular traction force field can be obtained by measuring the beads' displacement field. Since the TFM tracers are affected non-locally by the cellular traction field, obtaining the traction forces in TFM is mathematically more complicated than the conversion between displacement and traction force for MPAD arrays. Both TFM and MPADs have advantages: TFM allows cells to grow on a continuous

substrate of variable stiffness with high probe particle densities. MPADs form a lattice of independent force probes underneath the cell. The effective stiffness of the substrate can be varied by changing the geometry of the individual microposts (Fu et al., 2010). Of course, like all techniques based on cell culture in two dimensions, TFM and MPADs cannot reproduce the 3D cellular environment. However, the challenges associated with 3D approaches to measuring cellular traction forces mean that the 2D techniques can be expected to continue to have utility for the foreseeable future.

The protocols described herein focus on applying active MPADS (AMPADs) (MPADs with embedded magnetic nanowires) to enable high-precision measurements of both cellular passive and active microrheology rather than the static traction force or cells' response under large-scale external mechanical perturbations (Sniadecki et al., 2007; Trepats et al., 2007). A dual magnetic tweezer system actuates microposts with magnetic nanowires to measure local cellular rheology, while all the microposts serve as probes for measuring cellular fluctuations at high spatial and temporal resolution. Compared with other methodologies for performing cellular microrheology, AMPADs have the following advantages: first, compared with other active microrheology techniques, coating microposts tips with fibronectin enables controlled coupling of posts to cellular actomyosin network through focal adhesion; second, AMPADs provide an organized mapping of cytoskeletal fluctuations of different subcellular architectures with high spatial and temporal resolution. Moreover, compared with TFM, the independent nature of the micropost probes allows one to study their correlations, and the capability of embedding magnetic nanowires inside the microposts enables one to perform active and passive microrheology with the same system.

**Basic Protocol 1.** This protocol describes how to extend replica molding techniques for fabricating MPAD arrays (Fu et al., 2010; Yang et al., 2011) to embed magnetic Ni nanowires in individual microposts (Shi et al., 2019). The original work describing magnetic micropost array fabrication (Sniadecki et al., 2007; Sniadecki et al., 2008) used Co nanowires instead of Ni. While Co has a larger magnetic moment than Ni and hence can, in principle, provide larger magnetic actuation forces on individual microposts, some issues are associated with the use of Co that make Ni preferable. First, and most importantly, Co

metal dissolves in culture media and is toxic to cells. In the original work of Sniadecki et al., the larger micropost sizes used (4  $\mu\text{m}$  diameter) enabled the nanowires to be sufficiently well encased in the PDMS posts to minimize such issues. In contrast, Ni is not dissolved in culture media and is not measurably toxic in cell culture at the concentrations used in the experiments described here over the relevant exposure durations of a few days (Zhao, Boudou, Wang, Chen, & Reich, 2013). In addition, the magnetic properties of Co mean that Co nanowires do not form permanent magnets and so behave somewhat like superparamagnetic particles in a field perpendicular to their long axis (as one has here). As a result, microposts with Co nanowires can only be deflected in a single direction from their resting position, regardless of whether the applied magnetic field changes sign (Sniadecki et al., 2007; Sniadecki et al., 2008). Ni nanowires, in contrast, are good permanent magnets, so their actuation is bi-directional, following the direction of the applied field.

**Basic Protocol 2.** To optimize imaging of the microposts for the particle tracking analysis, this protocol employs imaging procedures that maximize both resolution and signal-to-noise while maintaining cell viability. Therefore, the microscope's condenser aperture is maximized to optimize resolution, and the illumination intensity is adjusted to maximize intensity in the captured frames without saturating the camera. The camera's digital gain is turned off to minimize camera noise. To capture bright-field movies at 100 fps, the exposure time is adjusted to 4.5 ms, so there is a gap in time between successive exposures to ensure no correlation between neighboring frames. To account for phototoxicity due to high illumination intensity, ultraviolet and infrared filters restrict the wavelength to  $425 \text{ nm} < \lambda < 700 \text{ nm}$ . The microscope's built-in green interference filter also helps to minimize photodamage. Post-tracking accuracy is extremely sensitive to focus drift and thermal fluctuations. An enclosed incubator and stage-mounted heating plate are used to keep the culture dish and its surroundings at  $37^\circ\text{C}$ . For long, multi-hour runs on the microscope to record force fluctuations for multiple cells, an on-stage environmental control chamber is used and filled with 5% premixed  $\text{CO}_2$  gas to help maintain cell viability. It is also important to allow sample dishes with cells on MPADs to stabilize at  $37^\circ\text{C}$  for 30 min in the enclosure prior to imaging to

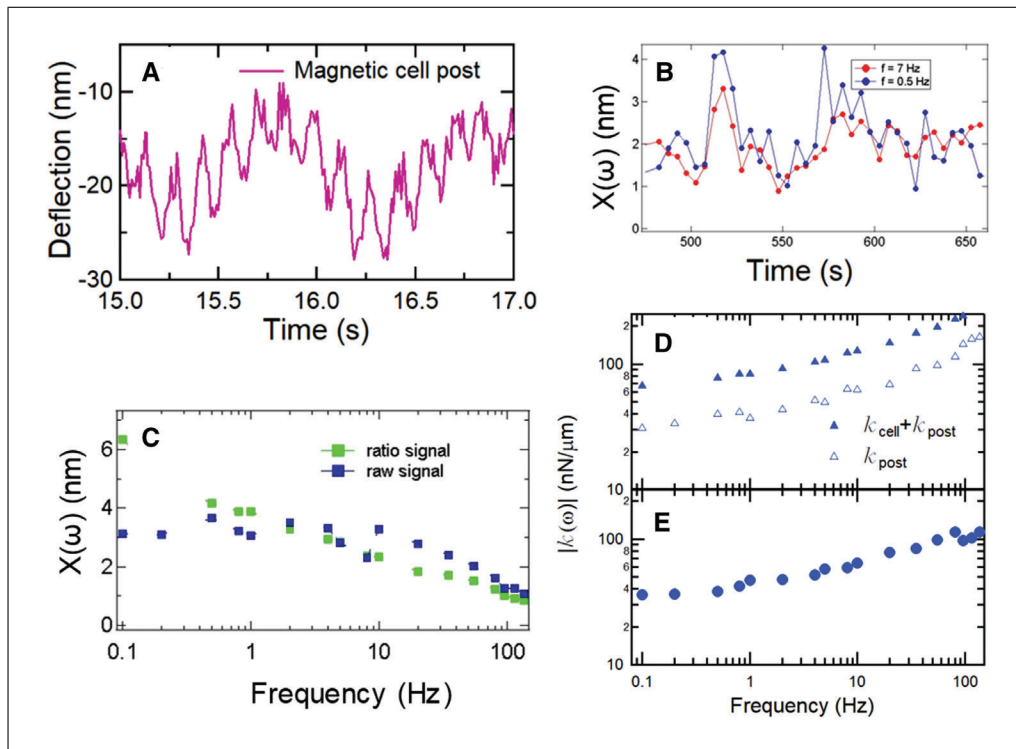


**Figure 31** Measurements of local cellular rheology with magnetic microposts. **(A)** Deflection of a cortex-adhered magnetic post, driven by a magnetic field with sinusoidal oscillations at a measurement frequency  $f = 1$  Hz and a reference frequency  $f_R = 7$  Hz. **(B)** The amplitudes of the responses at the two frequencies vary with time in a correlated way. **(C)** These temporal variations yield significant noise in the raw measurement of the post displacement amplitude  $x(\omega)$  (blue symbols). By calculating the ratio  $x(\omega)/x(\omega_R)$  (green symbols), this noise is greatly reduced, thus improving the determination of the frequency dependence of  $x(\omega)$ . **(D)** Frequency-dependent apparent stiffness of a post with a cell attached and the same post after removal of the cell. **(E)** Frequency-dependent cellular stiffness determined from the data in D.

minimize thermal fluctuations that can arise when transferring cell culture dishes from the culture incubator to the microscope stage.

**Basic Protocol 3.** Several experimental considerations must be addressed to acquire accurate data for the frequency dependence of the local cellular rheology with magnetic nanowires embedded in microposts and a magnetic tweezer system (Bose et al., 2018; Kramer, 2009; Lin et al., 2012; Zhao et al., 2014). To minimize evaporation and thermal fluctuations, we describe a customized sample chamber that allows the tips of the magnetic tweezer poles to be brought within 2 mm of the AMPAD array without contacting the culture media (Shi et al., 2019). This chamber greatly improves cell viability and decreases fluctuational noise in the measurements. A sinusoidal magnetic field results in micropost deflections of only a few nanometers. This does not interrupt normal cellular activity and keeps the measurements in the linear range. To account for time variance in the deflection magnitude associated with cellular activity (Massiera et al., 2007), such as time-dependent coupling

of the posts to the cytoskeleton, the actuating magnetic field is composed of a superposition of two frequencies: one frequency varies from 0.1 to 135 Hz to measure the frequency dependence of cellular stiffness, and the other is kept fixed (at 7 Hz in our case) to measure the time variance in deflection magnitude (Fig. 31A) (Shi et al., 2019). As the microposts themselves have a frequency-dependent viscoelastic response, after measuring the magnetic microposts' motion with cells attached, cells are removed, and the same field of view is measured again. By analyzing the differences between the magnetic posts' response with and without cells attached, one can extract the modulus of the cellular cortex (see Protocol 5).

**Basic Protocol 4.** To determine the microposts' positions versus time from the raw data (movies), Basic Protocol 4 implements a centroid-based particle tracking algorithm (Crocker & Grier, 1996) written in Igor Pro. Each frame is processed with a 2D Gaussian filter of 3 pixels full width at half maximum and an averaging filter with the micropost diameter. The results from the averaging

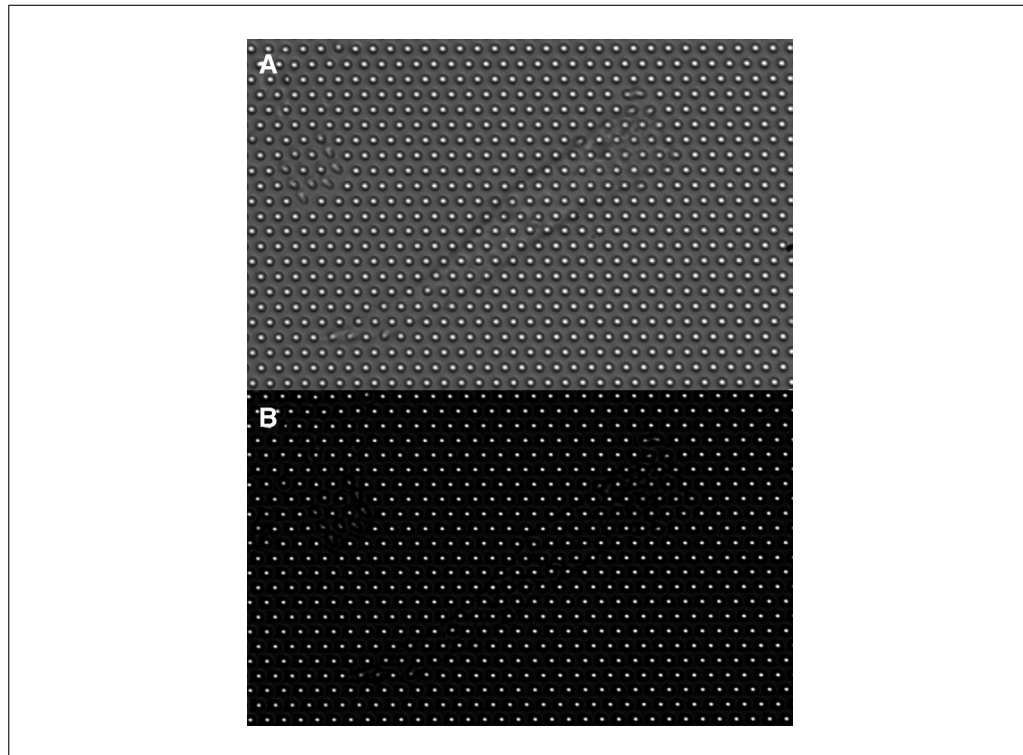


**Figure 32** (A) Raw image frame of micropost array. (B) Corresponding intermediate image following filtering as described in the Commentary.

filter are subtracted from the results from the Gaussian filter to obtain intermediate images with enhanced contrast and subtracted background (Fig. 32). A square mask is created, centered at the initial estimated position of the micropost center with a size slightly larger than the diameter of the micropost, and the center position is recalculated based on the intensity-weighted center of all pixels within the mask (centroid fitting). The mask is shifted toward the new fitted center by the closest integer number of pixels, and this process is repeated recursively until the difference between the center of the current mask and the fitted centroid is less than 0.5 pixels. To account for frame-to-frame drift, the average displacement in each frame relative to the movie's first frame of all the background microposts (those not in contact with cells) is subtracted from each micropost's trajectory. The undeflected positions of posts in contact with cells are determined by interpolation based on the positions of the background posts in the corresponding rows and columns of the array (Sniadecki et al., 2008).

**Basic Protocol 5.** The amplitudes and phases of the magnetic microposts' response at measurement frequency  $f$  and reference frequency  $f_R$  are found via digital lock-in analysis (Dixon & Wu, 1989) of the microposts' positions  $\mathbf{r}(t)$  determined from the image

sequences as described in Basic Protocol 4. Due to the finite exposure time, the AC amplitude extracted from the digital lock-in analysis is reduced in a frequency-dependent manner due to its averaging effect, as shown in the formula below.

Suppose we have a sinusoidal signal written as  $f(t) = A \cos \omega t$  (Equation 3). In our case,  $A$  is the deflection magnitude of the magnetic micropost, and  $\omega$  is the angular frequency of the magnetic field. Considering that the finite exposure time will give amplitude  $f(t)$  averaged over the exposure window, the recorded signal intensity  $S$  at the  $n^{\text{th}}$  frame recorded at frame rate  $\Delta t$  (see Equation 2) over finite exposure time  $T_e$  is

$$\begin{aligned}
 S &= \frac{1}{T_e} \int_{n\Delta t}^{n\Delta t + T_e} A \cos(\omega t) dt \\
 &= \frac{A}{T_e \omega} \{\sin[\omega(n\Delta t + T_e)] - \sin(\omega n\Delta t)\} \\
 &= \frac{2A}{\omega T_e} \sin \frac{\omega T_e}{2} \cos \left[ \omega \left( n\Delta t + \frac{T_e}{2} \right) \right] \\
 &= \frac{\sin \alpha}{\alpha} A \cos \left[ \omega \left( n\Delta t + \frac{T_e}{2} \right) \right]
 \end{aligned}$$

(Equation 4), where  $\alpha = \omega T_e/2$  (Equation 5). Therefore, the amplitude is reduced by a prefactor  $\frac{\sin \alpha}{\alpha}$  (Equation 6) and the phase is shifted by  $\alpha$ .

Another phase shift arises from the fixed lag time  $t_{lag}$  between the camera exposure window and the sampling of the magnetic field by the DAQ card. For our system, this is  $t_{lag} = 0.02$  s as measured by imaging an LED driven by the DAQ card.

Data at frequencies above the Nyquist frequency  $f_{Ny} = f_s/2 = 50$  Hz ( $f_s = 100$  Hz in our system) are measured via aliasing, i.e., at apparent frequencies  $f_k$ . Notably, this procedure will introduce an additional phase shift, as shown below:

Suppose a sinusoidal signal can be written as  $A = \cos(2\pi ft + \phi)$  (Equation 7), where  $f$  is the measured frequency and  $\phi$  is the phase shift. Since  $f_s t = n$  is the index of the frame captured by the camera, it is an integer. Then when  $50 \text{ Hz} < f < 100 \text{ Hz}$ ,

$$\begin{aligned} f_k &= f_s - f \\ S &= A \cos(2\pi ft + \phi) \\ &= A \cos(2\pi(f_s - f_k)t + \phi) \\ &= A \cos(2\pi f_s t - 2\pi f_k t + \phi) \\ &= A \cos(2\pi f_k t - \phi - 2\pi n) \\ &= A \cos(2\pi f_k t - \phi) \end{aligned}$$

(Equation 8).

This indicates that the phase is inverted from  $\phi$  to  $-\phi$  when measured at the apparent frequency  $f_k$  over the range  $50 \text{ Hz} < f < 100 \text{ Hz}$ . Similarly, when  $f > 100 \text{ Hz}$ ,

$$\begin{aligned} f_k &= f - f_s \\ S &= A \cos(2\pi ft + \phi) \\ &= A \cos(2\pi(f_s + f_k)t + \phi) \\ &= A \cos(2\pi f_s t + 2\pi f_k t + \phi) \\ &= A \cos(2\pi f_k t + \phi + 2\pi n) \\ &= A \cos(2\pi f_k t + \phi) \end{aligned}$$

(Equation 9).

Therefore, no additional phase is introduced when measured at the apparent frequency if  $f > 100 \text{ Hz}$ . All of these effects are accounted for in the Igor Pro code.

To estimate the resolution of the digital lock-in analysis, one can apply it to all microposts (magnetic and non-magnetic) under an AC magnetic field. We have found that the measured amplitudes of non-magnetic microposts are all  $< 0.5 \text{ nm}$ , which we have taken as our AC amplitude resolution  $\delta r < 0.5 \text{ nm}$  in our system.

To account for observed temporal fluctuations in  $x(\omega)$  (Fig. 31B), one calculates the ratio

$$x(\omega) = \frac{x_s(\omega)}{x_R(\omega_R)} \bar{x}_R(\omega_R)$$

(Equation 10) (Massiera et al., 2007), where  $x_s(\omega)$  is the response at the variable frequency  $f$  and  $x_R(\omega_R)$  is the response at the reference frequency  $f_R$  over the same measurement interval. The ratio of these signals is multiplied by  $\bar{x}_R(\omega_R)$ , the average of  $x_R(\omega_R)$  over all the measurement intervals, to keep the average of  $x(\omega)$  unchanged. This ratiometric approach yielded greatly reduced fluctuations in  $x(\omega)$  compared with those in  $x_s(\omega)$  (Fig. 31C).

The magnetic force  $F(\omega)$  is determined from the measured magnetic field  $B(\omega)$ , using the nanowires' magnetic moment and the nanowires' and microposts' dimensions (Sniadecki et al., 2008). The equivalent stiffness is then calculated as  $k(\omega) = F(\omega)/x(\omega)$  (Equation 11). Post stiffness  $k_{post}(\omega)$  is determined from data obtained after removing the cells by trypsinization, and the resulting cell stiffness is computed as  $k_{cell}(\omega) = k(\omega) - k_{post}(\omega)$  (Equation 12) (Fig. 31D). See also (Shi et al., 2019). Note that this effectively views the cell and the post as two viscoelastic units in parallel.

**Basic Protocol 6.** Due to the nature of bright field imaging, it is difficult to observe the cell edges accurately. However, one can use the calculated mean square displacement (MSD) of the microposts' trajectories to distinguish cell-associated posts from background posts. To obtain an accurate estimation of the MSD exponents  $\alpha$ , MSDs were fitted by a power law in the form of  $MSD = C + D\tau^\alpha$  (Equation 13) for  $\tau \leq 1$  s, and the constant  $C$  is subtracted from the MSDs as their noise floor estimation. The code calculates the logarithmic derivatives of the subtracted MSDs over lag time as

$$\frac{d \log(MSD_{Sub})}{d \log \tau}$$

(Equation 14)

and uses the averaged value over the range  $5 \text{ s} \leq \tau \leq 10 \text{ s}$  as the estimation for the MSD exponents (Fig. 33). By examining microposts far from cells, we have found that their MSD exponents  $\alpha$  are mostly less than 0.5 and use this criterion to distinguish background from cell posts.

Since cells can migrate on microposts over the typical 30-min time course of experiments using this technique, this protocol includes

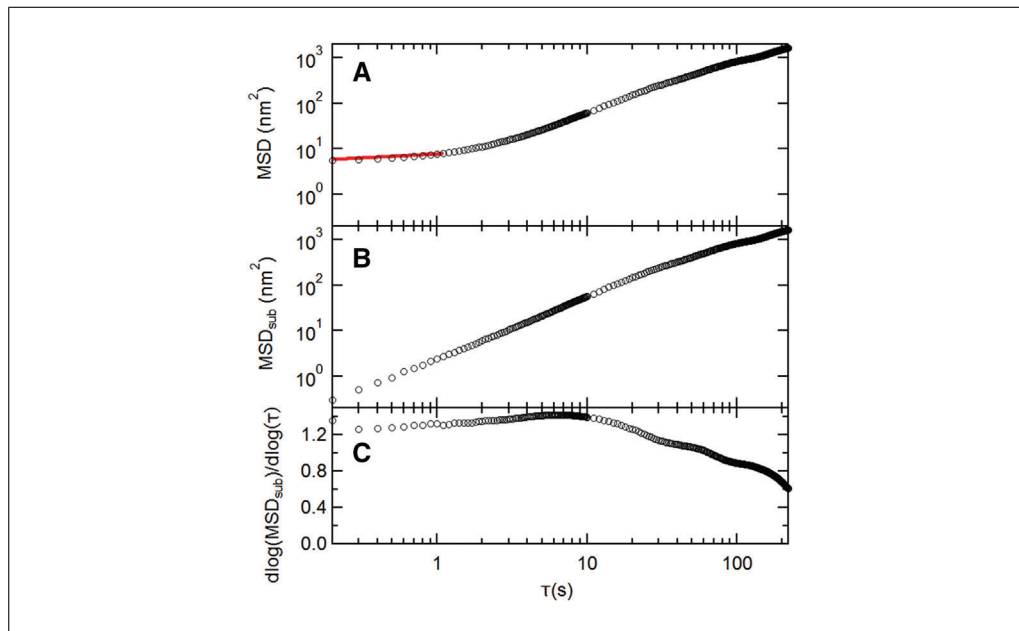


**Figure 33** Subtracted MSD and its logarithmic time derivative, illustrating the determination of the MSD exponent  $\alpha$  for two microposts. **(A)** Raw MSD traces showing fits (red lines) to determine the noise floor as described in the Commentary. **(B)** MSD traces  $MSD_{Sub}$  after subtracting the noise floor from the raw MSDs. **(C)** Logarithmic time derivatives of  $MSD_{Sub}$ . The MSD exponent  $\alpha$  and its uncertainty were obtained from the average of the logarithmic time derivative in the range  $5 \text{ s} \leq \tau \leq 10 \text{ s}$ . The MSDs were computed at 0.1 s intervals in  $\tau$ , but above  $\tau = 10 \text{ s}$ , they are only plotted every 1 s.

a procedure to identify posts associated with the cell for the full measurement interval. The trajectory of each post is broken up into three equal segments (10 min for a 30-min video), and the MSD exponent is calculated for each segment over the lag time range of 5-10 s as described above (where MSD and lag time follows a power-law relationship). To analyze cell-associated posts, we only accepted those with the first third and last third having  $\alpha > 0.5$ . Examples of how this criterion is applied are shown in Figure 34.

### Critical Parameters

Making the magnetic micropost arrays:

1. Ensure proper nanowire density. An excessively dense solution may result in excess nanowires in the micropost array base (not in the posts themselves), which will hinder imaging. A density that is too low may make it difficult to find cells with associated magnetic microposts.
2. In the magnetic actuation experiments (Basic Protocol 5), one must re-locate the former positions of the cells after they have been removed to re-measure the magnetic microposts' motion without the cells attached. Therefore, it is desirable to have reference marks of some kind in the micropost arrays to aid navigation. In arrays without such marks, it is usu-

ally best to work near the edge of the array and use the small but inevitable number of missing or collapsed posts (Fig. 35) as navigation aids to locate the magnetic posts.

Cell seeding on the arrays:

1. Seeding density should be set as described in the protocol, with sufficient cells but not enough to overlap.
2. Cells should be well spread on the microposts. When appropriate substrate stiffnesses are chosen, one can generally find microposts at the cell's periphery that are visibly bent, indicating good focal adhesion formation and mechanical contact between the cells and the microposts.

Obtaining high-quality images:

1. Image quality is crucial to ensuring the precision of localizing the post centers. This protocol maximizes illuminator intensity without photodamaging the cells. A sample image is shown in Figure 32A, where there is a clear contrast between the microposts' tops and the background while ensuring that the microposts' tops are as bright as possible without saturating the camera.

### Troubleshooting

Common problems with the protocols, their causes, and potential solutions are itemized in Table 1.

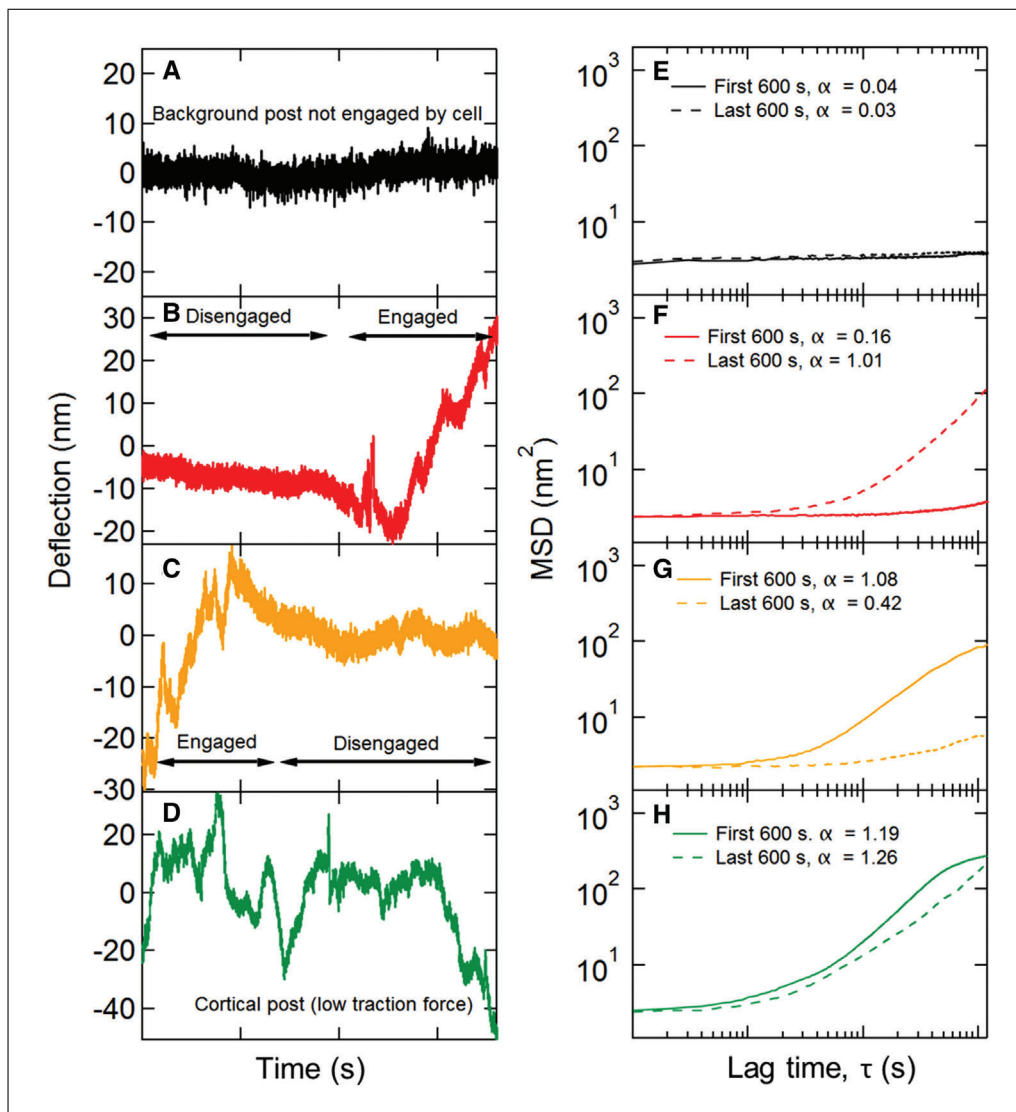


**Figure 34** Effects of cell motility on micropost dynamics and identification of microposts that were engaged with a cell over the full 1800 s measurement interval as those whose MSD exponents  $\alpha_1$  and  $\alpha_3$  computed over the first and final thirds of the trajectory, respectively, both be  $>0.5$  (A) A “background” micropost that was not in contact with the cell. (B) A micropost engaged with the cell only in the latter part of the measurement interval. (C) A micropost initially engaged with the cell, but subsequently released. (D) A micropost coupled to the cellular cortex throughout the measurement. (E-H) MSDs for the first and final thirds of the measurement intervals for the traces shown in A-D.

## Understanding Results

**Basic Protocol 1** should yield arrays of microposts with approximately 1% of the posts containing magnetic nanowires. An example of a portion of an array is shown in Figure 34. The “magnetic posts” are not always easy to spot with an optical microscope but frequently appear darker than the non-magnetic posts. Such a post is shown in the green circle in Figure 34. Note that when the concentration of nanowires is too high, the nanowires can become embedded in the base of the array between the microposts rather than within microposts. It can also be useful when initially fabricating magnetic post arrays to

collect images of several arrays by scanning electron microscopy. The nanowires show up clearly, and their presence can be verified by energy-dispersive x-ray (EDX) compositional analysis (Sniadecki et al., 2007; Sniadecki et al., 2008).

**Basic Protocol 2.** After incubation on the MPADs, cells should spread and adhere to the posts and exert traction forces on them (see Fig. 3). Observation of such forces has been widely discussed in the extensive literature on measuring quasi-static cellular traction forces with MPADs (Geng & Wang, 2016). In the imaging mode used here, details of the cells are not visible, but the outlines can usually be

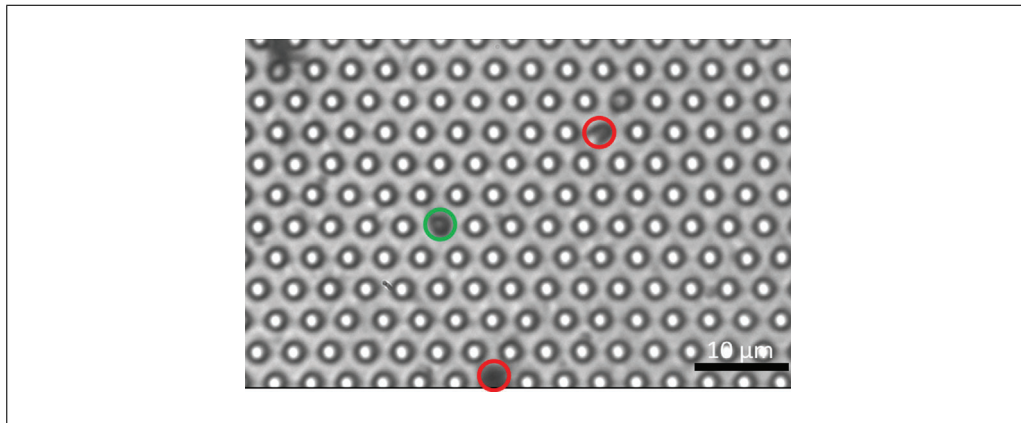


**Figure 35** Sample field of view for magnetic microposts array. The green circle indicates the location of a magnetic micropost. The two red circles indicate collapsed posts that can be used as navigation aids to trace back to the same location after cell removal.

**Table 1** Troubleshooting MPAD Fabrication and Data Collection

Problem	Possible Cause	Solution
Microposts collapsed	Microposts were allowed to dry, and forces from liquid evaporation caused posts to collapse.	Avoid letting the microposts dry out after submerging in liquid. If microposts are already collapsed, one can submerge them in ethanol and sonicate for 30 min.
No visible microposts with nanowires	Nanowire solution density too low	Increase nanowire solution density and/or increase volume of nanowire solution.
Nanowires inside base of MPAD array.	Nanowire solution density too high	Decrease nanowire solution density and/or decrease volume of nanowire solution.
Large drift/vibration when imaging cells on MPADs.	Air bubbles beneath coverglass	Remove air bubbles from beneath coverglass when loading MPADs into dish.
Focus drift over the time course of imaging.	System not in equilibrium	Wait for ~30 min before measuring the first cell.

observed with practice. If sufficient traction forces are being exerted by the cells, highly deflected posts near the edges of the cells can be seen (Fig. 3). The main output of this protocol is movies of the time dependence of the fluctuating cellular forces. The fluctuations in the microposts' positions are typically too small to observe by eye but are readily resolved with the image analysis techniques described in Basic Protocol 4.

**Basic Protocol 3** will yield data for the motion of the magnetic microposts under AC actuation. For larger actuations, this motion can be seen by the human eye (Supplementary Movie 1), but for local rheology measurements, the AC deflection amplitudes should be kept in the <10 nm range to remain linear. Such deflections are too small to see by eye but are readily detected upon image analysis

(see Fig. 26). Movies should be obtained with cells attached to the posts and after removal of the cells to enable subtraction of the contribution from the viscoelasticity of the posts themselves. To find the same region after cell removal, we use a naming convention to indicate the approximate location of the ROI on the micropost array when the cell is taken (for example, we name cell “TLTRc1” if the cell is taken at the top right corner of the top left quadrant of the microposts array), then use nearby imperfections in the micropost array to fine-tune its location. Examples of such movies are provided in the SI.

**Basic Protocol 4.** The data reduction in this protocol proceeds in three stages. These are illustrated below using selections from the output from the “PlotALot” function in the associated analysis code, allowing one to view the



x and y components of the posts' trajectories and their MSDs (after finishing MSD analysis in Basic Protocol 6). The initial centroid-based particle tracking analysis of the image sequences (the "Fit All Posts" function in the main GUI (see Fig. 14)) yields the "raw" x and y positions of each post in each video frame in the pixel coordinates of the camera (Fig. 36). Note that the three background posts in Figure 36 have remarkably similar trajectories. This reflects the background "drift" motion of the array. The amplitude of this motion of  $\sim 0.1$  pixels (12.5 nm) is comparable to the motion of the less active cell posts (e.g., Posts 277 and 278 in Fig. 36), which illustrates the need for the dedrifting procedure (the "Calc\_bgshift" function). The result of the dedrifting, which subtracts the average displacement of the background posts relative to the first frame, is illustrated in Figure 37. Note that the background posts' residual trajectories, with amplitudes of  $\sim 0.01$  pixels (1.2 nm), are reduced by approximately a factor of 10 compared to the raw data. Finally, after subtracting each post's undeflected position from the trajectory (via the CalcGrid-Center function), one obtains the deflection of each post versus time (Fig. 38) (still in pixels). These can be converted into distance from the measured array lattice constant and into force if desired from the posts' effective spring constant for lateral deflections (Fu et al., 2010). An example of this conversion is shown for the x-component of the motion for one cell post and one background post from Figures 36-38 in Figure 39. Note that analysis of the background data such (Fig. 38) yields information on the background noise for the cell posts in such measurements. In our studies, which include slight non-linearities in the mapping from physical location to centroided position, the dedrifting background post motion over 30-min observations was  $\sim 2$ -3 nm RMS when measured at 10 fps, which is small compared to the typical movement of cell-associated posts.

**Basic Protocol 5.** The oscillation of a magnetic post in response to the two-frequency, sinusoidal, driving magnetic field yields post motions such as that shown in Figure 31A, where the oscillations at both frequencies can be seen over the experimental noise. Such oscillations show considerable time dependence in their amplitudes. An example of this time dependence is shown in Figure 30B, in which significant noise is produced in the measurements of the response  $x(\omega)$  (Fig. 31C,

raw signal). However, it is important to note that the amplitudes of the responses at the two frequencies are correlated in time, an effect that can be attributed to time dependence in the cell's coupling to the post (Massiera et al., 2007). Thus, a significant reduction in the uncertainty of the frequency dependence of  $x(\omega)$  is obtained by the ratiometric analysis described above (Fig. 31C, ratio signal). The frequency-dependent stiffness of the cell + post  $k(\omega) = F(\omega)/x(\omega)$  (Fig. 31D) is determined from  $x(\omega)$  and the magnetic force. The stiffness of the post alone  $K_{\text{post}}(\omega)$  is determined by remeasuring the response of the post alone (Fig. 31D), and then the final result  $k_{\text{cell}}(\omega)$  is determined from the difference between these two measurements (Fig. 31E).

**Basic Protocol 6.** The measurements of cellular fluctuations (Basic Protocols 2 and 4) yield time traces of the displacements of the microposts in contact with a cell, such as the examples shown in Figures 39 and 30A. Such fluctuating motion is typically characterized in terms of its mean square displacement (MSD)  $\langle \Delta r^2(\tau) \rangle = \langle (\mathbf{r}(t+\tau) - \mathbf{r}(t))^2 \rangle$  (Equation 13), where  $\tau$  is the lag time. Examples of typical MSDs for individual posts are shown in Figure 30B. These data display a noise floor at short  $\tau$  and then power-law behavior, with the  $\text{MSD} \propto \tau^\alpha$  for 1-2 decades in  $\tau$ . This power-law exponent is typically  $> 1$ , with larger values for posts near the periphery of the cell. To ensure sufficient data are available for the MSDs, one should only compute the MSDs for  $\tau$  up to  $\sim 1/5$  of the video length. To measure the MSD exponent  $\alpha$  for each post, the software in Protocol 6 first obtains a post's noise floor by fitting the MSD trace for  $\tau \leq 1$  s to the form  $\text{MSD} = C + D\tau^\alpha$  (Equation 15), and then subtracts the constant  $C$  from the MSD traces to obtain the "subtracted MSD,"  $\text{MSD}_{\text{Sub}}$ . It then calculates the logarithmic time derivative  $\frac{d \log(\text{MSD}_{\text{Sub}})}{d \log \tau}$  (Equation 16), and averages between  $5 \text{ s} \leq \tau \leq 10 \text{ s}$  to obtain  $\alpha$  and its uncertainty (see Fig. 33). Figure 34 illustrates the identification of posts associated with a cell throughout the measurement window by requiring that such posts show  $\alpha > 0.5$  for both the first and last third of their trajectories (based on the observation that background posts show  $\alpha < 0.5$ ). This example shows a background post for reference, two posts engaged with the cell for only part of the measurement, and one that is engaged throughout the measurement. The corresponding MSDs for the first and last thirds of the measurement illustrate the cut based on  $\alpha$ .

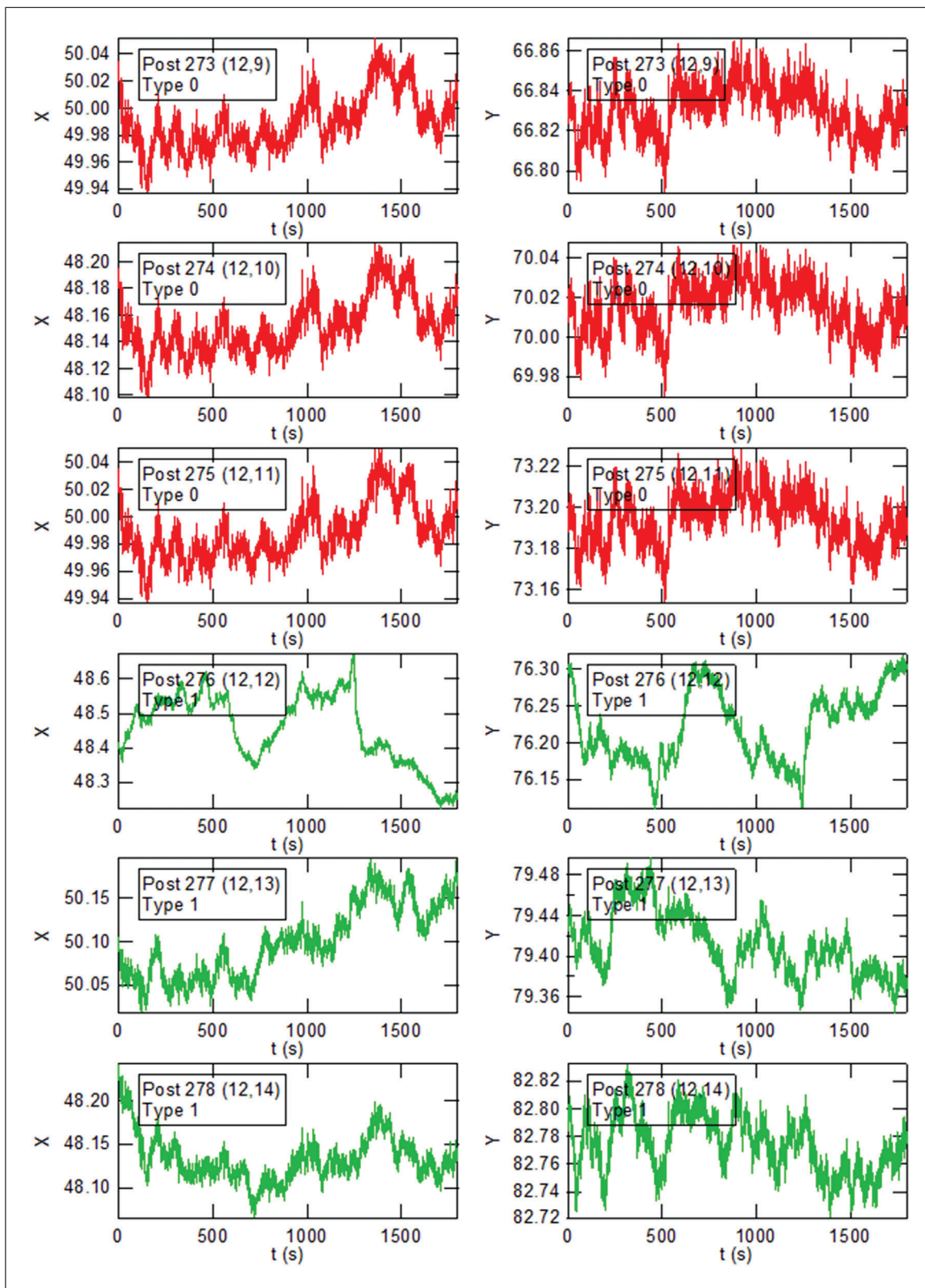


**Figure 36** Raw post trajectory data. X (left column) and Y (right column) coordinates (in camera pixels) of selected posts as determined from particle tracking analysis versus time (in seconds). In these data, 1 pixel = 125 nm. This video was taken at 10 fps, and so includes 18,000 time points. These plots are generated by the “Plot-a-lot” function in the associated IgorPro analysis code. The post number is that in the Igor data arrays, and the (a,b) notation references a representation of the hexagonal post lattice in a 2D array. Post type 0 (red) denotes background posts, and Post type 1 (green) denotes cell-associated posts.

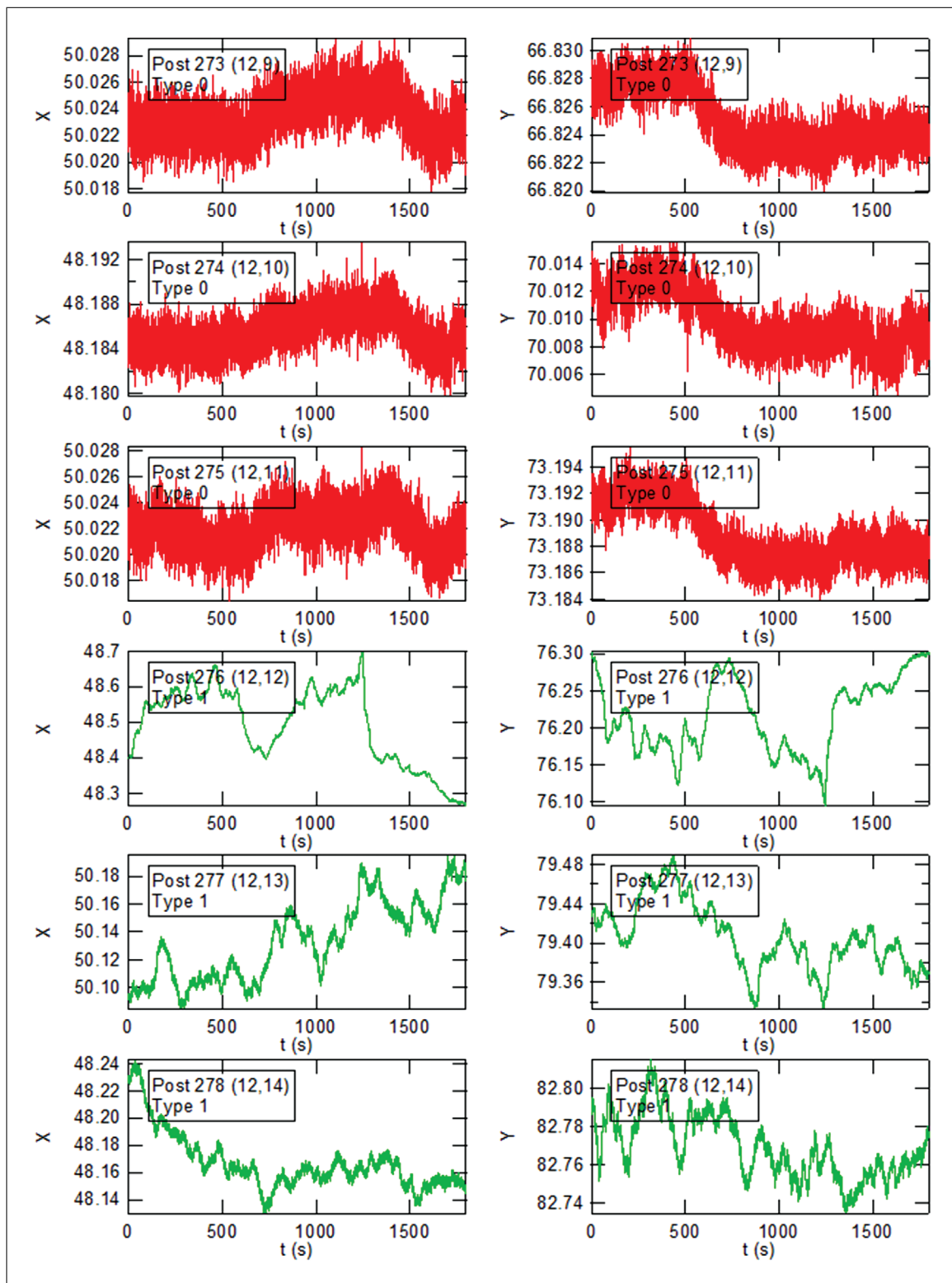


**Figure 37** Dedrifted post trajectory data. X (left column) and Y (right column) coordinates (in camera pixels) of the posts shown in Figure 33 following dedrifted versus time (in seconds). In these data, 1 pixel = 125 nm. This video was taken at 10 fps, and so includes 18,000 time points. The plots are generated with the “Plot-a-lot” function in the associated IgorPro analysis code. The post number is that in the Igor data arrays, and the (a,b) notation references a representation of the hexagonal post lattice in a 2D array. Post type 0 (red) denotes background posts, and Post type 1 (green) denotes cell-associated posts.

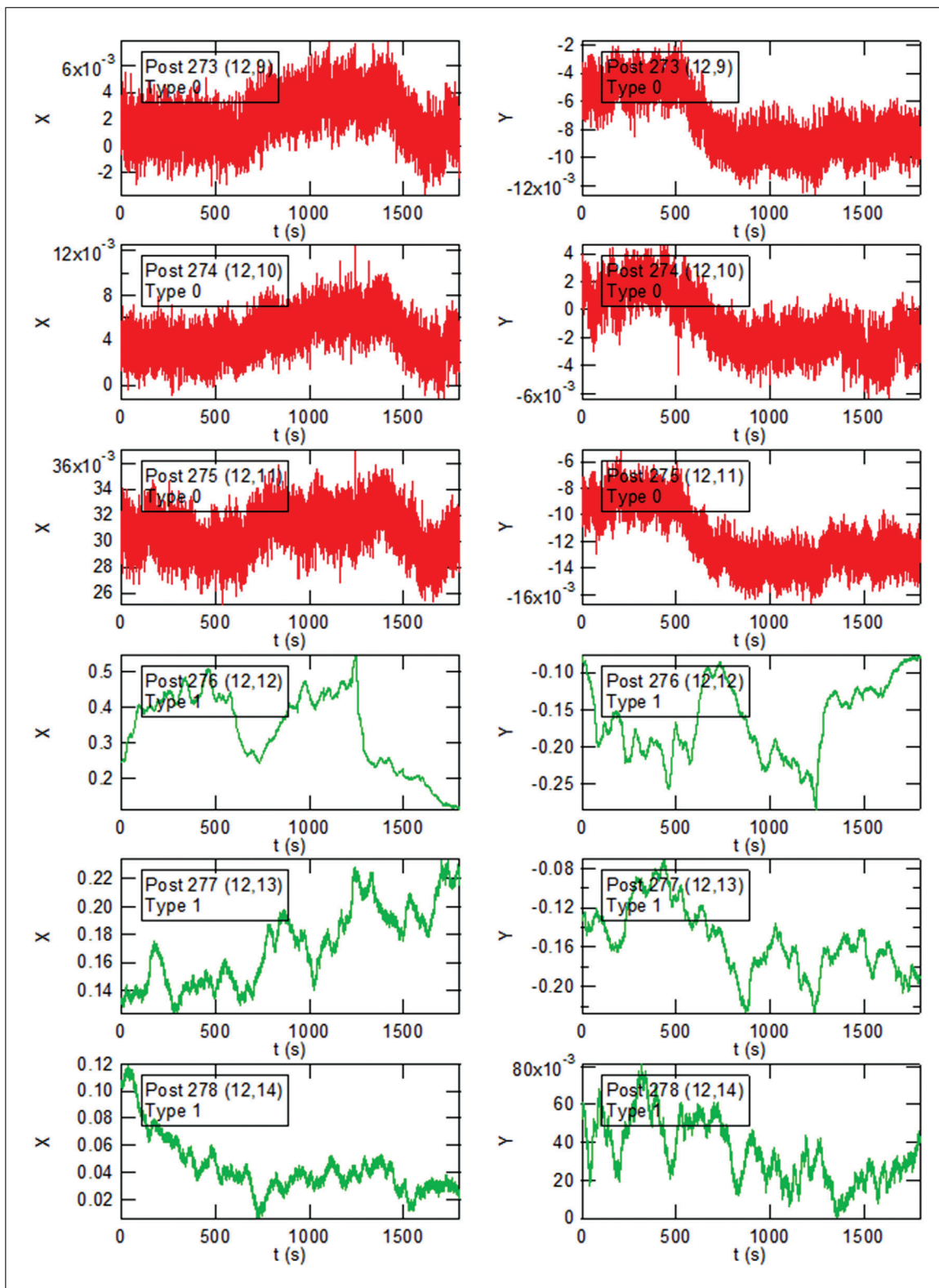


**Figure 38** Micropost deflection data. X (left column) and Y (right column) coordinates (in camera pixels) versus time (seconds) of the posts shown in Figures 33 and 34 following subtraction of the individual posts' undeflected positions. In these data, 1 pixel = 125 nm. This video was taken at 10 fps, and so includes 18,000 time points. The plots are generated with the "Plot-a-lot" function in the associated IgorPro analysis code. The post number is that in the Igor data arrays, and the (a,b) notation references a representation of the hexagonal post lattice in a 2D array. Post type 0 (red) denotes background posts, and Post type 1 (green) denotes cell-associated posts.

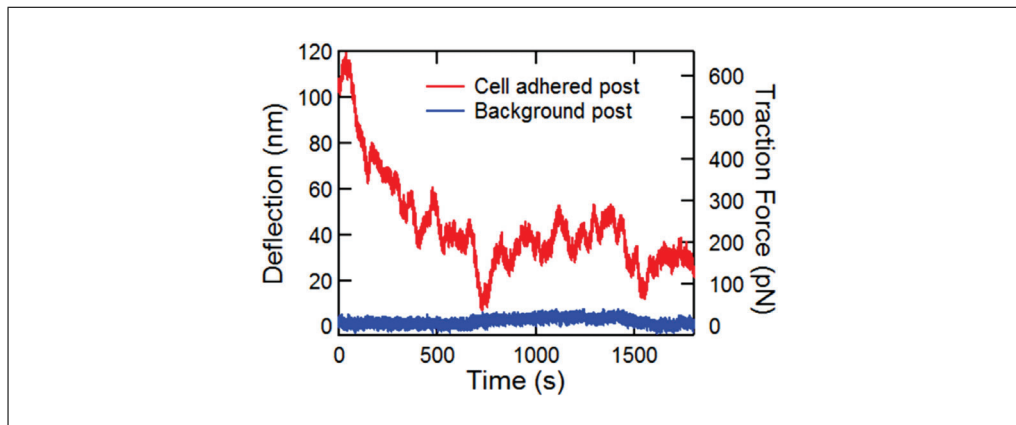


**Figure 39** X-component of deflection data in nm versus time for cell post 278 and background post 273 from Figure 33. The right-hand vertical axis shows the conversion to traction force, based on the posts' spring constant  $k = 15.7 \text{ nN}/\mu\text{m}$ .

A key output of this protocol is the production of spatial maps of the MSD exponent (see Fig. 30C) and magnitude (see Fig. 30D). The output of the Basic Protocol 6 software that identifies sets of posts associated with stress fibers and the actomyosin cortex based on the posts' average traction force is illustrated in Figure 30E-G. Here, for cells on microposts with spring constant  $k = 15.7 \text{ nN}/\mu\text{m}$ , we identify the posts as stress fiber-associated if their average traction forces are larger than 5 nN, and as cortical posts if their maximum traction force is less than 2 nN. This bifurcation procedure provides clean data sets that can form the basis for subsequent analysis of cytoskeletal dynamics. We have used such data to study cytoquake phenomena and other aspects of cytoskeletal fluctuations (Shi et al., 2019; Shi et al., 2021).

### Time Considerations

In Basic Protocol 1, embedding nanowires into micropost molds takes approximately 2-3 hr. The majority of this time is waiting for the ethanol to evaporate from the nanowire solution. Casting PDMS in molds takes 30 min, followed by baking overnight. Fabrication of magnetic nanowires takes about 30 min to set up, and the electrodeposition takes 20-30 min. Extracting nanowires takes about 1 hr of the operator's time and 12-18 hr of wait time.

In Basic Protocol 2, cell seeding takes approximately 30 min, then the cells adhere and spread on the posts overnight. Imaging takes 10-20 min to set up the microscope and optimize imaging parameters and 30 min for settling to thermal equilibrium. The actual imaging time then depends on the length of observation desired. For half-hour observations per cell, it is typically possible to measure 7 to 8 cells from a single substrate in a single day.

In Basic Protocol 3, setting up the Streampix script takes about 15 min. Microscope setup (including setting up magnetic tweezers and optimizing image parameters) takes about 30 min. Each cell takes about 30 min to scan across all frequencies from 0.1 to 135 Hz.

In Basic Protocol 4, setting up the grid for localizing micropost centers and creating hand-drawn cell masks takes about 10 min per cell. For 17 videos taken at 100 fps from 3 min to 30 s (following the recording script described in Basic Protocol 4) with  $\sim 1000$  posts ( $30 \times 30$  grid, approximately the whole ROI of our CCD camera when using a  $40\times$  objective), it will take 10 hr to analyze on a Dell Precision Tower 5810 PC.

In Basic Protocol 5, digital lock-in calculations of all micropost trajectories across all frequencies take about 30 min. Calculating the rheology curve of magnetic microposts takes about 5 min.

In Basic Protocol 6, MSD calculations take about 1 hr on the aforementioned data (180,000 frame videos). Generating a mask of cell-associated posts based on MSD exponents takes 30 min, and bifurcating cortical and stress fiber-associated posts takes about 5 min.

### Acknowledgments

This work was supported by the National Heart, Lung and Blood Institute of the National Institutes of Health grant number HL-127087, and the National Science Foundation grant PHY-1915193 at Johns Hopkins University, and by the National Science Foundation grant PHY-1915174 at the University of Pennsylvania. We thank C. S. Chen for providing MPAD masters.

## Author Contributions

**Yu Shi:** Conceptualization, Formal analysis, Investigation, Methodology, Software, Validation, Visualization, Original draft, review, and editing; **Shankar Sivarajan:** Investigation, Software, Validation, Visualization, Original draft, review, and editing; **John C. Crocker:** Conceptualization, Formal analysis, Funding acquisition, Investigation, Methodology, Project administration, Supervision, Original draft, review, and editing; **Daniel H. Reich:** Conceptualization, Data curation, Formal analysis, Funding acquisition, Methodology, Project administration, Software, Supervision, Original draft, review, and editing.

## Conflict of Interest

The authors declare no conflict of interest.

## Data Availability Statement

The data, tools, and material (or their source) that support the protocol are available from the corresponding author upon reasonable request.

## Literature Cited

- Alencar, A. M., Ferraz, M. S. A., Park, C. Y., Millet, E., Trepate, X., Fredberg, J. J., & Butler, J. P. (2016). Non-equilibrium cytoquake dynamics in cytoskeletal remodeling and stabilization. *Soft Matter*, *12*(41), 8506–8511. doi: 10.1039/c6sm01041e
- Bose, P., Huang, C. Y., Eyckmans, J., Chen, C. S., & Reich, D. H. (2018). Fabrication and mechanical properties measurements of 3D microtissues for the study of cell-matrix interactions *Methods in Molecular Biology*, *1722*, 303–328. doi: 10.1007/978-1-4939-7553-2\_18
- Crocker, J. C., & Grier, D. G. (1996). Methods of digital video microscopy for colloidal studies. *Journal of Colloid and Interface Science*, *179*(1), 298–310. doi: 10.1006/jcis.1996.0217
- Dixon, P. K., & Wu, L. (1989). Broad-band digital lock-in amplifier techniques. *Review of Scientific Instruments*, *60*(10), 3329–3336. doi: 10.1063/1.1140523
- du Roure, O., Saez, A., Buguin, A., Austin, R. H., Chavrier, P., Siberzan, P., & Ladoux, B. (2005). Force mapping in epithelial cell migration. *Proceedings of the National Academy of Sciences*, *102*(7), 2390–2395. doi: 10.1073/pnas.0408482102
- Fabry, B., Maksym, G. N., Butler, J. P., Glogauer, M., Navajas, D., & Fredberg, J. J. (2001). Scaling the microrheology of living cells. *Physical Review Letters*, *87*(14), 148102. doi: 10.1103/PhysRevLett.87.148102
- Felton, E. J. (2009). *Applications of magnetic nanostructures to cell patterning and heterotypic cell-cell interactions*. (Ph.D. Ph.D.). Johns Hopkins University, Baltimore.
- Floyd, C., Levine, H., Jarzynskie, C., & Pa-poian, G. A. (2021). Understanding cytoskeletal avalanches using mechanical stability analysis. *Proceedings of the National Academy of Sciences of the United States of America*, *118*(41), e2110239118. doi: 10.1073/pnas.2110239118
- Fu, J. P., Wang, Y. K., Yang, M. T., Desai, R. A., Yu, X. A., Liu, Z. J., & Chen, C. S. (2010). Mechanical regulation of cell function with geometrically modulated elastomeric substrates. *Nature Methods*, *7*(9), 733–736. doi: 10.1038/nmeth.1487
- Geng, Y. X., & Wang, Z. J. (2016). Review of cellular mechanotransduction on micropost substrates. *Medical and Biological Engineering and Computing*, *54*(2-3), 249–271. doi: 10.1007/s11517-015-1343-2
- Guo, M., Ehrlicher, A. J., Jensen, M. H., Renz, M., Moore, J. R., Goldman, R. D., ... Weitz, D. A. (2014). Probing the stochastic, motor-driven properties of the cytoplasm using force spectrum microscopy. *Cell*, *158*, 822–832. doi: 10.1016/j.cell.2014.06.051
- Hecht, F. M., Rheinlaender, J., Schierbaum, N., Goldmann, W. H., Fabry, B., & Schaffer, T. E. (2015). Imaging viscoelastic properties of live cells by AFM: Power-law rheology on the nanoscale. *Soft Matter*, *11*(23), 4584–4591. doi: 10.1039/c4sm02718c
- Hoffman, B. D., Massiera, G., Van Citters, K. M., & Crocker, J. C. (2006). The consensus mechanics of cultured mammalian cells. *Proceedings of the National Academy of Sciences of the United States of America*, *103*(27), 10259–10264. doi: 10.1073/pnas.0510348103
- Hultgren, A., Tanase, M., Chen, C. S., & Reich, D. H. (2004). High-yield cell separations using magnetic nanowires. *IEEE Transactions on Magnetics*, *40*(4), 2988–2990. doi: 10.1109/TMAG.2004.830406
- Hultgren, A., Tanase, M., Felton, E. J., Bhadriraju, K., Salem, A. K., Chen, C. S., & Reich, D. H. (2005). Optimization of yield in magnetic cell separations using nickel nanowires of different lengths. *Biotechnology Progress*, *21*(2), 509–515. doi: 10.1021/bp049734w
- Kilpatrick, J. I., Revenko, I., & Rodriguez, B. J. (2015). Nanomechanics of Cells and Biomaterials Studied by Atomic Force Microscopy. *Advanced Healthcare Materials*, *4*(16), 2456–2474. doi: 10.1002/adhm.201500229
- Kramer, C. M. (2009). *Probing the dynamics of cellular traction forces with magnetic and non-magnetic micropost arrays*. (Ph.D. Ph.D.). Johns Hopkins University, Baltimore.
- Lau, A. W. C., Hoffman, B. D., Davies, A., Crocker, J. C., & Lubensky, T. C. (2003). Microrheology, stress fluctuations, and active behavior of living cells. *Physical Review Letters*, *91*(19), 198101. doi: 10.1103/PhysRevLett.91.198101
- Li, M., Dang, D., Liu, L. Q., Xi, N., & Wang, Y. C. (2017). Atomic force microscopy in characterizing cell mechanics for biomedical applications: A review. *Ieee Transactions on*

- Nanobioscience*, 16(6), 523–540. doi: 10.1109/Tnb.2017.2714462
- Lin, Y. C., Kramer, C. M., Chen, C. S., & Reich, D. H. (2012). Probing cellular traction forces with magnetic nanowires and microfabricated force sensor arrays. *Nanotechnology*, 23, 075101. doi: 10.1088/0957-4484/23/7/075101
- Lohner, J., Rupprecht, J. F., Hu, J., Mandriota, N., Saxena, M., Pitta de Araujo, D., ... Sheetz, M. P. (2019). Large and reversible myosin-dependent forces in rigidity sensing. *Nature Physics*, 15, 689–695. doi: 10.1038/s41567-019-0477-9
- Martino, F., Perestrelo, A. R., Vinarsky, V., Pagliari, S., & Forte, G. (2018). Cellular Mechanotransduction: from tension to function. *Frontiers in Physiology*, 9, 824. doi: 10.3389/fphys.2018.00824
- Massiera, G., Van Citters, K. M., Biancaniello, P. L., & Crocker, J. C. (2007). Mechanics of single cells: Rheology, time dependence, and fluctuations. *Biophysical Journal*, 93(10), 3703–3713. doi: 10.1529/biophysj.107.111641
- Mohammed, D., Versaavel, M., Bruyere, C., Alaimo, L., Luciano, M., Verduyssen, E., ... Gabriele, S. (2019). Innovative tools for mechanobiology: Unraveling outside-in and inside-out mechanotransduction. *Frontiers in Bioengineering and Biotechnology*, 7, 162. doi: 10.3389/fbioe.2019.00162
- Plotnikov, S. V., Sabass, B., Schwarz, U. S., & Waterman, C. M. (2014). High-resolution traction force microscopy. *Quantitative Imaging in Cell Biology*, 123, 367–394. doi: 10.1016/B978-0-12-420138-5.00020-3
- Rovner, J. B. (2013). *The static and dynamic properties of colloidal inclusions in nematic liquid crystals*. (Ph.D. Ph.D.). Johns Hopkins University, Baltimore.
- Shi, Y. (2020). *Dissecting cytoskeletal dynamics with active micropost arrays*. (Ph.D. Ph.D.). Johns Hopkins University, Baltimore.
- Shi, Y., Porter, C. L., Crocker, J. C., & Reich, D. H. (2019). Dissecting fat-tailed fluctuations in the cytoskeleton with active micropost arrays. *Proceedings of the National Academy of Sciences*, 116(28), 13839–13846. doi: 10.1073/pnas.1900963116
- Shi, Y., Sivarajan, S., Xiang, K. M., Kostecky, G. M., Tung, L., Crocker, J. C., & Reich, D. H. (2021). Pervasive cytoquakes in the actomyosin cortex across cell types and substrate stiffness. *Integrative Biology*, 13(10), 246–257. doi: 10.1093/intbio/zyab017
- Smith, B. A., Tolloczko, B., Martin, J. G., & Grutter, P. (2005). Probing the viscoelastic behavior of cultured airway smooth muscle cells with atomic force microscopy: Stiffening induced by contractile agonist. *Biophysical Journal*, 88(4), 2994–3007. doi: 10.1529/biophysj.104.046649
- Sniadecki, N. J., Anguelouch, A., Yang, M. T., Lamb, C. M., Liu, Z., Kirschner, S. B., ... Chen, C. S. (2007). Magnetic microposts as an approach to apply forces to living cells. *Proceedings of the National Academy of Sciences*, 104(37), 14553–14558. doi: 10.1073/pnas.0611613104
- Sniadecki, N. J., Lamb, C. M., Liu, Y., Chen, C. S., & Reich, D. H. (2008). Magnetic microposts for mechanical stimulation of biological cells: Fabrication, characterization, and analysis. *Review of Scientific Instruments*, 79(4), 044302. doi: 10.1063/1.2906228
- Tan, J. L., Tien, J., Pirone, D. M., Gray, D. S., Bhadriraju, K., & Chen, C. S. (2003). Cells lying on a bed of microneedles: An approach to isolate mechanical force. *Proceedings of the National Academy of Sciences of the United States of America*, 100(4), 1484–1489. doi: 10.1073/pnas.0235407100
- Tanase, M., Felton, E. J., Gray, D. S., Hultgren, A., Chen, C. S., & Reich, D. H. (2005). Assembly of multicellular constructs and microarrays of cells using magnetic nanowires. *Lab on a Chip*, 5(6), 598–605. doi: 10.1039/B500243E
- Trepatt, X., Deng, L. H., An, S. S., Navajas, D., Tschumperlin, D. J., Gerthoffer, W. T., ... Fredberg, J. J. (2007). Universal physical responses to stretch in the living cell. *Nature*, 447(7144), 592–595. doi: 10.1038/nature05824
- Wei, M. T., Zaorski, A., Yalcin, H. C., Wang, J., Hallow, M., Ghadiali, S. N., ... Ou-Yang, H. D. (2008). A comparative study of living cell micromechanical properties by oscillatory optical tweezers. *Optics Express*, 16(12), 8594–8603. doi: 10.1364/OE.16.008594
- Weng, S. N., & Fu, J. P. (2011). Synergistic regulation of cell function by matrix rigidity and adhesive pattern. *Biomaterials*, 32(36), 9584–9593. doi: 10.1016/j.biomaterials.2011.09.006
- Wolfenson, H., Meacci, G., Liu, S. M., Stachowiak, M. R., Iskratsch, T., Ghassemi, S., ... Sheetz, M. P. (2016). Tropomyosin controls sarcomere-like contractions for rigidity sensing and suppressing growth on soft matrices. *Nature Cell Biology*, 18(1), 33–42. doi: 10.1038/ncb3277
- Yang, M. T., Fu, J. P., Wang, Y. K., Desai, R. A., & Chen, C. S. (2011). Assaying stem cell mechanobiology on microfabricated elastomeric substrates with geometrically modulated rigidity. *Nature Protocols*, 6(2), 187–213. doi: 10.1038/nprot.2010.189
- Zhao, R., Boudou, T., Wang, W. G., Chen, C. S., & Reich, D. H. (2013). Decoupling cell and matrix mechanics in engineered microtissues using magnetically actuated microcantilevers. *Advanced Materials*, 25(12), 1699–1705. doi: 10.1002/adma.201203585
- Zhao, R., Boudou, T., Wang, W. G., Chen, C. S., & Reich, D. H. (2014). Magnetic approaches to study collective 3D cell mechanics in long-term cultures (invited). *Journal of Applied Physics*, 115, 172616. doi: 10.1063/1.4870918

## Internet Resources

The Streampix module files and Igor Pro procedure files needed to run experiments and analyze data are available on Github at <https://github.com/yushi1898/MPAD-Analysis-Code>.